3. TECHNOLOGY PROGRAMME

3. Technology

The technology activities carried out by the Euratom-ENEA Association in the framework of the European Fusion Development Agreement concern the Next Step (International Thermonuclear Experimental Reactor - ITER), the Long-Term Programme (breeder blanket, materials, International Fusion Materials Irradiation Facility - IFMIF), Power Plant Conceptual Studies and Socio-Economic Studies. The Underlying Technology Programme was set up to complement the fusion activities as well to develop technologies with a wider range of interest.

The Technology Programme mainly involves staff from the Frascati laboratories of the Fusion Technical and Scientific Unit and from the Brasimone laboratories of the Advanced Physics Technologies Unit. Other ENEA units also provide valuable contributions to the programme. ENEA is heavily engaged in component development/testing and in design and safety activities for the European Fusion Technology Programme. Although the work documented in the following covers a large range of topics that differ considerably because they concern the development of extremely complex systems, the high level of integration and coordination ensures the capability to cover the fusion system as a whole.

Programme

In 2004 the most significant testing activities concerned the ITER primary beryllium-coated first wall. In the field of high-heat-flux components, an important achievement was the qualification of the process for depositing a copper liner on carbon fibre composite (CFC) hollow tiles. This new process, pre-brazed casting (PBC), allows the hot radial pressing (HRP) joining procedure to be used also for CFC-based armour monoblock divertor components. The PBC and HRP processes are candidates for the construction of the ITER divertor. In the materials field an important milestone was the commissioning of a new facility for chemical vapour infiltration/deposition, used for optimising silicon carbide composite (SiC_f/SiC) components. Eight patents were deposited during 2004. Many design activities involving neutron, electromagnetic and thermal-mechanical computations were performed for the Joint European Torus (JET) and ITER. Significant contributions were also made to the studies on safety and environment, the Power Plant Conceptual Design and socio-economics.

The most relevant activities and the main results are documented in the following sections.

3.2.1 ITER divertor

Manufacturing of small-scale tungsten monoblock mockups. The work on manufacturing a prototype component by using hot radial pressing (HRP) continued (Underlying Technology and EFDA contract 03/1054). A new CFC//Cu joining technique (pre-brazed casting [PBC]) was also developed and successfully applied in manufacturing the CFC monoblock components. Finite-element (FE) analyses were used to simulate the thermal-mechanical behaviour of the CFC material under HRP conditions, taking into account the anisotropic properties and low mechanical strength of CFC. A "compressing rig" was designed and manufactured according to the FE calculations performed to simulate the temperature transient and inner tube pressure and considering the fact that the CFC tiles have to be mechanically contained to avoid failure of the material. A small mockup with three CFC tiles tested under thermal fatigue cycling (fig. 3.1) withstood, after intermediate loading steps, up to 1000 cycles at 25 MW/m^2 without incurring damage. The HRP technique was also successfully used to manufacture a small curved mockup with four tungsten tiles. The next step will be to use HRP to manufacture the 250-mm prototypical component with both CFC and tungsten armour. The prototype consists of a high-heat-flux unit with a straight CFC monoblock segment and a curved tungsten monoblock segment, attached to a steel supporting structure. The roughly 250-mm-long cooling tube is made of CuCrZr [3.1-3.5].

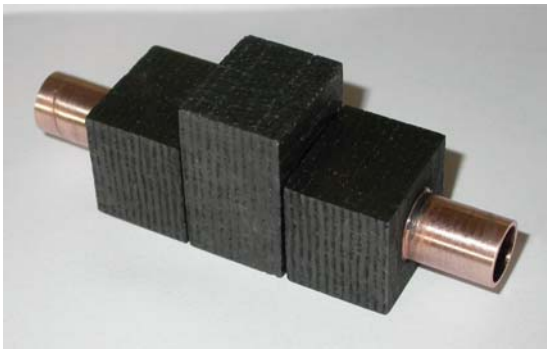

Fig. 3.1 - Monoblock mockup with three CFC tiles after HRP manufacturing

Integration and hydraulic tests of full-scale ITER divertor components. The activity involves identifying and preparing all the procedures needed to perform the assembly and integration of the ITER divertor components on a cassette body, as well as the definition of the experimental thermal hydraulic tests on the draining and drying of a full-scale prototype to be manufactured (EFDA contract 02/682). Theoretical analyses of the flow distribution and pressure drop in each cooling channel of each component were concluded in mid-2004. The steady-state hydraulic behaviour of the cassette and its plasma-facing components (PFCs) was investigated by means of the MS-Excel model and the RELAP5 code. The RELAP5 model (fig. 3.2) also permits analyses of flow distributions and can be used for the transient calculation of the cassette draining procedures. Estimation of the total pressure drop between the I/O manifolds by MS-Excel and RELAP5 resulted in values of 1.28 and 1.27 MPa, respectively, at the nominal flow rate of 17.3 kg/s for each cassette assembly; the overall hydraulics were, respectively, P(MPa)=5.55×10^{-3} G 1.90514 (kg/s) and P(MPa)=5.02×10^{-3} G 1.92560 (kg/s). Although cooling of the whole divertor assembly by a serial flow organisation with different and complicated PFC geometries was considered a challenge, the solutions adopted meet all the design requirements: i) pressure drop lower than the design value (1.4 MPa); ii) adequate margins against the occurrence of the critical heat flux (>40%); iii) acceptable flow distortion in the draining-loop tubes (<20%). For maintenance purposes, each cassette will be drained of the residual internal water and then dried. Due to the complex pipe geometry, discharge by gravity is incomplete, but compressed gas, supplied through the cooling channels at appropriate input pressure and flow conditions, should cause rapid evacuation, without either bubbling in the vertical channels or separated streams in the horizontal channels.

Fig. 3.2 - RELAP5: geometrical model of ITER divertor

During draining the water coolant at atmospheric pressure is blown out at 4.5 MPa by N_2 injected in the inlet manifolds. The results obtained with the codes confirm that evacuating the divertor cassette by gas blowing would be possible. Experimental comparisons will contribute both to assessing this procedure and to qualifying the RELAP5 code for specific fusion-relevant applications.

Characterisation of plasma-facing materials. Two of the four samples of W and W + 1% Al_2O_3 macrobrush, provided by the European Fusion Development Agreement (EFDA), were exposed to the FTU boundary plasma by means of the sample-introduction system and characterised (task TPP-ERTUBE-D3) by scanning electron microscopy (SEM) and x-ray diffraction (XRD) analyses (fig. 3.3). Because of parasitic exposure during other experimental campaigns, strong plasma-sample interaction sometimes led to overheating and consequent melting of the samples, with an unpredictable loss of retained deuterium. The remaining samples will be exposed to mild discharges. The recently available optical multichannel analyser will allow both the deuterium and the tungsten flux to be monitored. Due to the crowded FTU experimental programme and the shutdown at the end of October 2004, the contract has been extended by six months (up to June 2005).

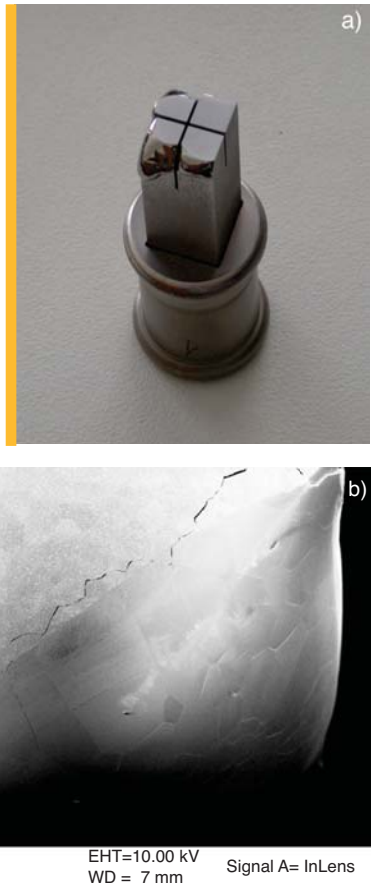

Fig. 3.3 - a) Tungsten sample after exposure in the FTU scrape-off layer; b) SEM image of the molten zone

3.2.2 ITER first wall

Qualification tests on Engineering Design Activity (EDA) mockups. The qualification of the small mockups (DS12I, DS8J, DS2I [manufactured by FRAMATOME France] and DS 10J [manufactured by NNC Ltd. UK]) representative of the ITER primary first wall (EFDA contract 00/529–task FW-MUFT) continued under the EDA III test campaign. Mockup DS2I was a dummy spare element representing a first wall without Be tiles. The same base fabrication route was used for all the mockups, but the joining of the Be tiles to the DS-Cu (Glidcop-Al25) heat-sink support was performed under different hot isostatic pressing (HIP) conditions to check the corresponding thermal fatigue behaviour. Mockup DS10J had already been tested during EDA I for a total of 50 fatigue cycles with the heat flux up to 0.32 MW/m^2 and during EDA II for a total of 180 fatigue cycles up to 0.50 MW/m^2; mockup DS8J, during EDA II for a total of 180 fatigue cycles up to 0.5 MW/m^2. Nondestructive examination (NDE) by ultrasonic tests performed by FRAMATOME before EDA III excluded any defects at the Be-Cu alloy HIP joints. The four mockups were assembled on an appropriate frame and housed inside the EDA-BETA. Thermocouples (ANSI K) were positioned on the back of the mockups at different depths from the first wall, in the Cu alloy layers and in some Be tiles. The results of a

References

[3.1] M. Merola et al., Fusion Eng. Des. **56-57**, 173 (2001)

[3.2] M. Roedig et al., Fusion Eng. Des. **56-57**, 417 (2001)

[3.3] M. Roedig et al., *Investigation of tungsten alloys as plasma facing materials for the ITER divertor*, Proc. 6th Int. Symp. on Fusion Technology – ISFNT-6 (San Diego 2002)

[3.4] E. Visca et al., Fusion Eng. Des. **56-57**, 343 (2001)

[3.5] M. Roedig et al., *Post irradiation testing of samples from the irradiation experiments, PARIDE 3 and PARIDE 4*, 11th Int. Conf. on Fusion Reactor Materials (Kyoto 2003)

Fig. 3.4 - EDA III mockup assembly after 8244 fatigue cycles – lateral view without resistor

campaign to monitor current dispersion to the ground, evaluate the efficiency of heat transfer between resistor and mockups and validate the ANSYS code calculation demonstrated the excellent behaviour of the facility.

The task had the initial aim of reaching a total of 30000 fatigue cycles up to 0.80 MW/m^2 at the reference fatigue period of 300 s. During the test preparation EFDA decided to reduce the maximum superficial heat flux to 0.65 MW/m^2, keeping the reference period at 300 s, so the tests were performed (at the reference period) with 60 s of linear ramp-up, 180 s at constant power and 60 s of linear ramp-down.

Continuous monitoring of the current dispersion to the ground demonstrated that this value always remained below 2 mA when the current to each arm of the resistor was about 1000 A. No electric arc discharge between the resistor and the mockup assembly was recorded. In August 2004, the EDA III test campaign was suspended after having reached 8244 fatigue cycles, divided as follows: 4126 fatigue cycles (5-40 kW - 300 s), corresponding to a heat flux of 0.05-0.43 MW/m^2; 4118 fatigue cycles (15-60 kW - 300 s), corresponding to a heat flux of 0.16-0.65 MW/m^2. In September, after the decision to stop EDA III and launch EDA IV with a different mockup assembly, final dismantling was started. No failures, melting or detachments were found for any of the Be tiles (fig. 3.4). DS12I was further examined prior to sending it back to the FRAMATOME for final US inspection. The CFC electric resistor was still in good condition, with only limited graphitization on its surface. After mounting the new mockup assembly and preliminary testing, the EDA IV test campaign was launched at the beginning of November 2004.

First-wall inspection. The aim of the activity (EFDA contract 03/1113) is to assess whether the ITER wide-angle viewing/thermography system can supplement other systems, in particular visible/infrared spectroscopy. The completion date was extended by six months (to July 2005) because of the extension of the Commissariat à l'Energie Atomique (CEA) task related to the activity. In 2004 work was devoted to

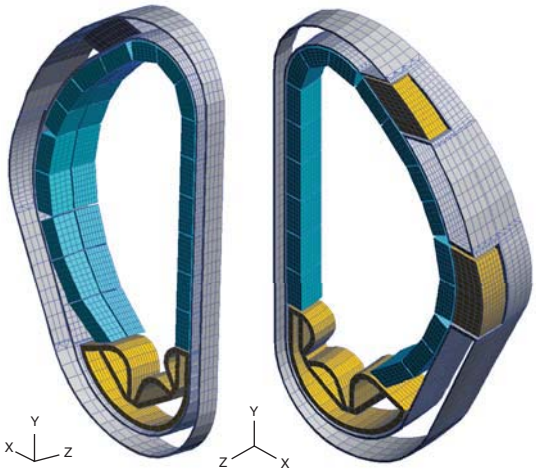

Fig. 3.5 - Coarse model (full 3D elements) of a 10° ITER sector including one half (two counter-faced halves) of the shielding blanket modules at the inboard (at the outboard), the double shell vessel and the main features of the upper and equatorial ports

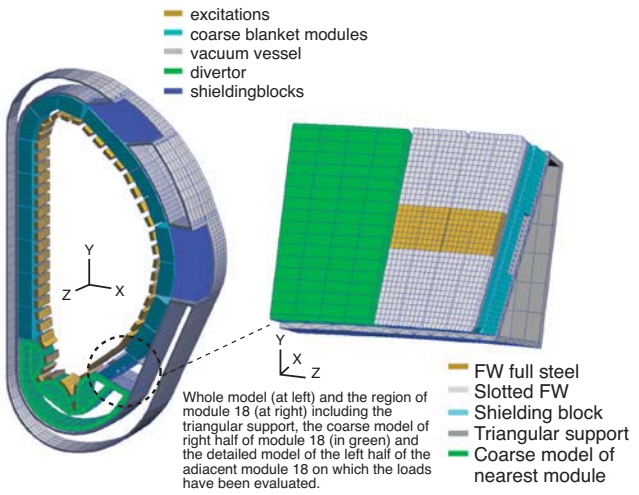

Fig. 3.6 - ITER model (EMAS code) after modifications made to accommodate the detailed model of module 18

reviewing the visible/infrared spectroscopy and first-wall inspection requirements and to preliminary calculation of the system "etendue" needed to meet the requirements.

3.2.3 Electromagnetic analysis of ITER blanket

The electromagnetic (em) loads during plasma disruptions on the ITER shielding blanket modules were evaluated. A special technique was adopted to overcome the difficulties in modelling extremely small details in a very large structure. A course 3D finite-element method (FEM) model of a 10° toroidal sector of ITER was developed (fig. 3.5) and then used to determine the boundary conditions for detailed analyses of each single component. Some of the analyses (for the upper port plug, electron cyclotron resonance heating launcher and module 18) have already been performed. Detailed models of some of the components are shown in figure 3.6. The main results are summarised in the tables 3.I and 3.II. All the data were obtained with the FEM em code EMAS. The most severe disruption was used as excitation load in analysing each component. The 10° toroidal sector was also modelled with the em module of the ANSYS code in order to have an alternative and more flexible numerical tool. The model was run with simplified excitation (a pure central disruption lasting 40 ms) and the results compared with those of the coarse EMAS model. The ANSYS and EMAS results are in quite satisfactory agreement, while in terms of computer performance the ANSYS code, considering the different number of degrees of freedom in the two models, seems to be more advantageous than EMAS.

Table 3.I - Main results of em analyses of the upper plug assembly. Excitation load: upward VDE (linear current quench of 40-ms duration)

Torque point: x(radial)=11.687; y(vertical)=5.467; z=0 - geometric centre of the port end - load components in ITER global reference frame

M_g(MNn)	M_y(MNm)	M_z(MNm)	F_x(MN)	F_y(MN)	F_z(MN)
-1.15	-0.25	-0.1	0.07	0.04	0.093

Table 3.II - Main results of em analyses module 18

A: Excitation load: downward VDE (18-ms exponential current quench decay time)

Torque point: geometric centre of the module (m): x(radial)=7.248; y(vertical)=2.893; z=0

Load components in local reference frame

M_{rad}(MNn)	M_{pol}(MNm)	M_{tor}(MNm)	F_{rad}(MN)	F_{pol}(MN)	F_{tor}(MN)
-0.3	-0.035	-0.015	0.002	0.001	0.003

Reaction forces from support housing and stub keys

Reaction force from support housing (MN)	Reaction force from stub keys (MN)
0.2	0.26

B: Excitation load: downward VDE (40-ms linear current quench) moment relative to geometric centre between attachments

Moment relative to geometric centre between attachments

TMM (0.676)	-0.32	0.46	-0.02	0.000	-0.02	-0.01

Reaction forces from support housing and stub keys

Reaction force from support housing (MN)	Reaction force from stub keys (MN)
0.41	0.31

3.3.1 Liquid breeder blanket

Water-cooled lithium-lead (WCLL) blanket. Work on tritium kinetics in the WCLL blanket continued (task TTBA-004-D1). In the second half of 2004 the experimental data from the SOLE and LEDI devices were used to develop a model of the behaviour of hydrogen in the eutectic alloy Pb-16Li. Literature data on diffusivity from Reiter and solubility from Wu were confirmed, and now a complete set of parameters is available for use in the design of the system for tritium extraction from Pb-16Li in the new helium-cooled lithium-lead blanket concept.

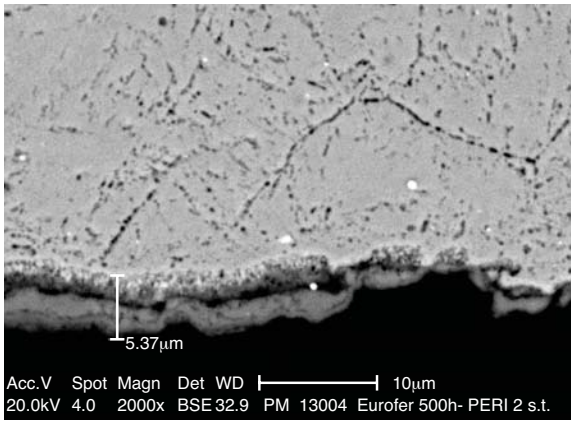

Fig. 3.7 - Surface micrograph of an oxidized specimen: the oxide layer produced by self-healing is evident

Helium-cooled lithium-lead (HCLL) blanket. The activity on the characterisation of coatings acting as permeation and/or corrosion barriers (task TTBC-003-D1) was concluded. In situ oxidation apparatus was used to verify the reliability of the self-healing effect. This procedure also showed that it is possible to maintain the starting permeation reduction factor (PRF) during operation. The PRF is strongly affected by the original pre-oxidation procedure, and in-situ oxidation simply repairs the damage to the original oxide layer through nucleation of an inner adherent oxide (fig. 3.7). In any case the PRF values obtained are high enough to allow the use of this technique for the HCLL blanket module.

Construction of the European Breeding Blanket Test Facility. The design of the loop was concluded in October 2003 and a new deliverable was assigned to ENEA for the construction of the facility (task TTBC-004-D1). A European call for tender was launched in October 2004, and the selection of primary firms was concluded in November 2004. The procedure is still ongoing and assignment of the contract is expected in February 2005. The facility will consist of a liquid metal loop to simulate the thermofluidodynamic conditions foreseen in the HCLL blanket concept; a He cooling circuit (He-FUS3); a gas circuit for injecting hydrogen/deuterium; an extractor to purge gas from liquid metal; instrumentation and a complete data acquisition and control system.

Flowing Pb-16Li corrosion on EUROFER steel. The experimental campaign was concluded in March 2004 after reaching a total exposure time of 6000 h (task TTBC-003-D3). The results reported in 2003 were confirmed, that is, a linear increase in corrosion, a constant corrosion rate of about 30 mm/y, and uniform corrosion with no preferential elemental depletion.

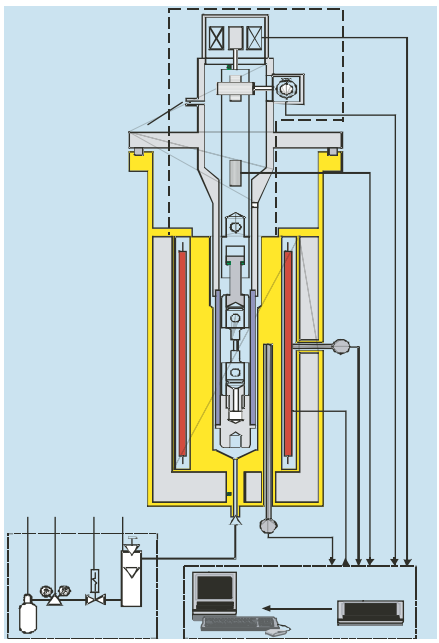

Fig. 3.8 - Tensile test machine for irradiated specimens

System for tritium recovery from Pb-16Li. Construction of the TRIEX loop started in July 2004, and the facility will be operative in April 2005 (task TTBC-004-D1). The original design was maintained, and a numerical simulation demonstrated the feasibility of the technical solutions adopted to extract hydrogen from liquid metal.

Mechanical properties of RAFM steels in Pb-16Li environment. A procedure was developed for investigating irradiation effects on the liquid metal embrittlement of the reduced-activation ferritic-martensitic (RAFM) steel EUROFER 97 in Pb-16Li alloy (task TTMS-003-6). Specimens for tensile testing, a capsule, a suspension system and the BOR-60 irradiation assembly were designed. The specimens were loaded in capsules filled with Pb-16% Li alloy. The assembly was irradiated in the BOR-60 reactor. The irradiation temperature varied from 315 to 332°C, and the damage dose was 0.26-5.9 dpa, depending on the location of the specimens in the core. Out-of-reactor tensile tests on the specimens have to be carried out in the same alloy. At present the irradiated specimens are being tested in a dedicated facility (fig. 3.8).

3.3.2 Solid breeder blanket

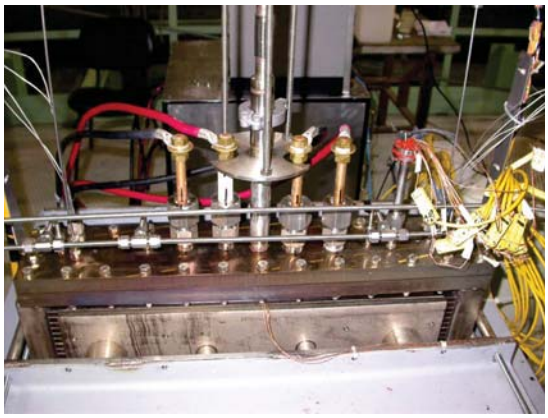

Fig. 3.9 - HELICA mockup under testing

HELICHETTA III test campaign. The campaign has further confirmed that both the Li_2TiO_3 and the Li_4SiO_4 pebble beds, when correctly filled in a rigid breeder cell containment and swept by helium purge flow, exhibit cyclically repetitive behaviour vs. the heat flux stepping ramp thermal behaviour (fig. 3.9). The goals of evaluating the reduction in bed height and the lateral load exerted during cycles were achieved. The pebble temperatures and measured lateral loads were mainly affected by the inhomogeneous mechanical and thermal (i.e., load cell temperature) boundary conditions, but the influence of the variation in bed packing, probably due to relocation of the pebbles in a vertical direction, cannot be excluded. The lateral loads were very low because the bed reduction allowed free expansion vertically. Although the fillings were done with high-frequency vibrations, the overall bed-height reduction was very evident for both Li_2TiO_3 and Li_4SiO_4 pebbles at the beginning of the thermal cycling, reaching saturation within around 20 cycles. Despite a noticeable overall reduction ranging from 1.6 to 4%, the beds showed very regular thermo-mechanical behaviour during the cycles, with few minor exceptions. Indeed, as the mockup operated in the vertical position, the bed-height reduction was not expected to have much effect on the efficiency of thermal exchange with the cooling/heating plates. At the end of each test, the pebbles were discharged by an air ejector and filtered in the range of 0.5 - 1 μm. Submicrometric powders were released, especially in the case of Li_4SiO_4.

Design of the new pebble-bed test blanket module mockup. The objective is out-of-pile testing of the helium-cooled pebble bed (HCPB) blanket mockups, in particular, simulation of the thermal-mechanical loads on the pebble beds and their relevant structures. The design of the new test blanket module (TBM) mockup to be tested in He-FUS3 is being developed under a collaboration between ENEA, Forschungszeuntrum Karlsruhe (FZK), CEA and EFDA. Fabrication of the TBM mockup has been assigned to CEA Grenoble.

The new TBM mockup will represent a 1/3 scale U-bend HIP simulacrum of the first wall with welded caps and stiffening plates, in a geometry (pebble-bed-layer thickness, cooling plate and first-wall dimensions, instrumental lead and piping feedthroughs) adapted to the experimental requirements. Steady-state and thermal cycling fatigue tests at the reference helium pressure, temperature and heat loads will be simulated by internal and external flat electrical heaters. The timing of the mockup fabrication has still to be precisely defined, but the first small-scale mockups should be available by early to mid-2005.

Ceramic Breeders. Work on the wet reprocessing of Li_2TiO_3 pebbles and the reprocessing of Li_2TiO_3 pebbles by a direct sol-gel route continued. The reprocessing of Li from ceramic Li_2TiO_3 breeder ceramics [3.6] was improved, using two routes. In the first the Li_2CO_3 was recovered by adding Na_2CO_3 to a solution obtained from Li_2TiO_3 pebbles and HNO_3 and then the precipitated powders were washed for Na impurities (fig. 3.10). The second route was developed in cooperation with the Japan Atomic Energy Research Institute (JAERI) under an International Energy Agency (IEA) programme. Li_2TiO_3 dissolution was performed in commercial H_2O_2 at room temperature, and a syrup based on citric Li-Ti-peroxide complexes was obtained [3.7]. The syrup was initially gelled by dropping it in cold acetone, but the particles obtained could not be sintered at a density >90% of

References

[3.6] C. Alvani et al., J. Nucl. Mater. **307-311**, 837 (2002); and J. Nucl. Mater. **289**, 303 (2001)

[3.7] S. Casadio et al., *Procedimento per il recupero di metatitanato di litio ceramico*, ENEA-JAERI Patent - Inv. Ind. N°BO2004A000428

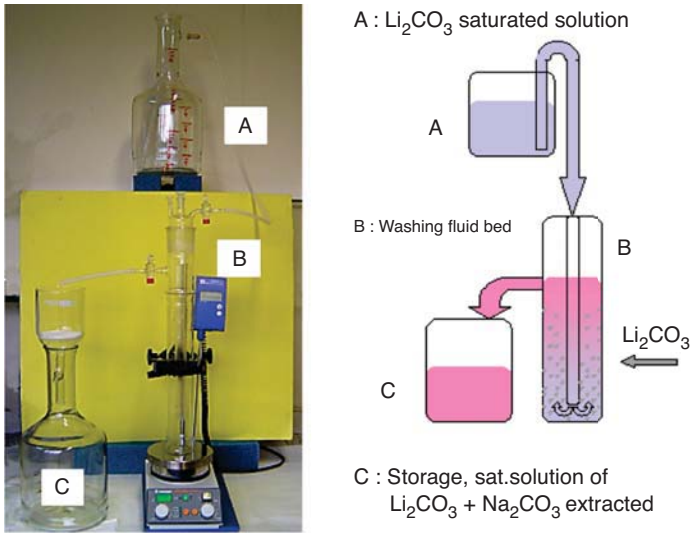

Fig. 3.10 - Schematic of the Li_2CO_3 washing stage

the theoretical density. However higher density was obtained from the dried – calcined - granulated syrup.

The effect of Li-depletion (due to Li-burn-up) on the chemical interaction between Li_2TiO_3 and He+0.1%H_2 (at 900°C) sweeping gas was studied under the IEA programme. Burn-up was chemically simulated by preparing and examining a large number of pellet and pebble specimens with a Li/Ti atomic ratio between the limits 0 (pure TiO_2) and 2 (pure Li_2TiO_3) and inducing a known fraction alpha of the $Li_4Ti_5O_{12}$ spinel phase.

3.3.3 Fuel cycle

Permeator tubes. Production of the thin-walled (500 mm long, 6 mm thick and 6 mm in diam) permeator tube was completed (task TTFD-TR31). The design of the permeator module of the PERMCAT reactor was modified in order to meet the safety requirements (minimum shell thickness of 3 mm) and to allow the catalyst filling procedure [3.8]. The main parts of the reactor (fig. 3.11) were constructed according to the new design.

Fig. 3.11 - Main parts of the PERMCAT reactor: palladium tube, metal bellows and reactor shell

The production of Pd-Ag membranes of reduced thickness and the use of metals alternative to palladium were also studied [3.9,3.10].

Vent detritiation system. The objective is to experimentally investigate the behaviour of the vent detritiation system (VDS) in the presence of smoke and combustion products generated by a fire occurring in an operating area of the tritium plant (task TTFD-TR49). Under heating, some plastics in the tritium laboratory burn or decompose by generating smoke as well as combustion products, such as hydrochloric and hydrofluoric acid, that can poison the catalyst and impair the detritiation process. The experimental plan for testing the catalysts, indicating the test parameters (gas

compositions, temperatures, exposure times, materials to be tested), has been worked out and the experimental apparatus designed. The efficiency of the VDS recombiner catalyst will be tested by reproducing a fire environment in a test cell and then measuring the efficiency by injecting some tritium, as a tracer, in the stream of smoke routed to the catalyst bed. The tritium concentration will be measured by the liquid scintillation technique in water samples [3.11].

3.4.1 ITER pre-compression ring material

Studies continued on the unidirectional fibreglass composite for the ITER pre-compression ring. Three further melts were produced, but the samples were not long enough to allow for the very high shear force and, as a result, the gripping tabs became detached before failure of the resistant section (fig. 3.12). A new mould was developed for manufacturing 600-mm-long samples [3.12].

3.4.2 ITER magnet casing design

Additional tests were performed at Ansaldo Superconduttori in order to find the maximum thickness of modified AISI 316LN (high nitrogen content) that could be electron-beam welded (EBW) without unacceptable defects (fig. 3.13). Limited-extent defects were found in welding 40-mm-thick samples, while unacceptable defects were found in 60-mm and 80-mm-thick samples. A study is in progress to find the parameters for welding 60 mm of steel.

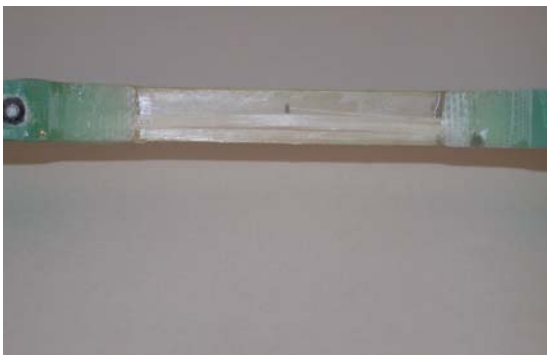

Fig. 3.12 - Collapsed sample of fibreglass

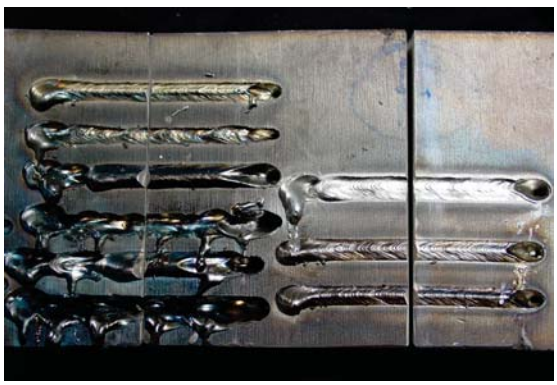

Fig. 3.13 - Melt runs performed on AISI stainless steel to set up the welding characteristics of the EBW machine at Ansaldo Superconduttori

References

[3.8] S. Tosti, L. Bettinali and D. Lecci, *Improvements to the mechanical design of the PERMCAT component construction of membrane tubes*, ENEA Internal Report FUS TN BB-R 007 (2004)

[3.9] S. Tosti, La Chimica e l'Industria, anno **86, 9**, 70 (2004)

[3.10] S. Tosti et al., J. Mater. Sci. **39**, 3041 (2004)

[3.11] C. Rizzello and S. Tosti, *Experimental investigation of vulnerability of VDS catalyst to poisoning by species released during fire*, ENEA Internal Report FUS TN BB-R 009 (2004)

[3.12] C. Nardi, L. Bettinali and A. Pizzuto, *Fiberglass unidirectional composite to be used for ITER pre-compression rings,* presented at the 23rd Symp. on Fusion Technology - SOFT-23 (Venice 2004)

3.4.3 High-frequency/high-voltage solid-state body power-supply for ITER gyrotrons

An innovative body power-supply (BPS) has been designed to modulate the voltage of the body of the ITER ECRH collector depressed potential (CDP) gyrotron [3.13] in the range 0-45 kV within a frequency band of 10 kHz. During 2004 the first module of the BPS was built and successfully tested at OCEM, Bologna, Italy (fig. 3.14). The BPS will be completed within 2005.

At the same time, the design of the solid-state modulator for the European CDP Gyrotron Test Facility progressed in collaboration with OCEM. ENEA was in charge of performing digital simulation of the entire system under normal and fault conditions and of supervising the manufacture of the BPS for the facility.

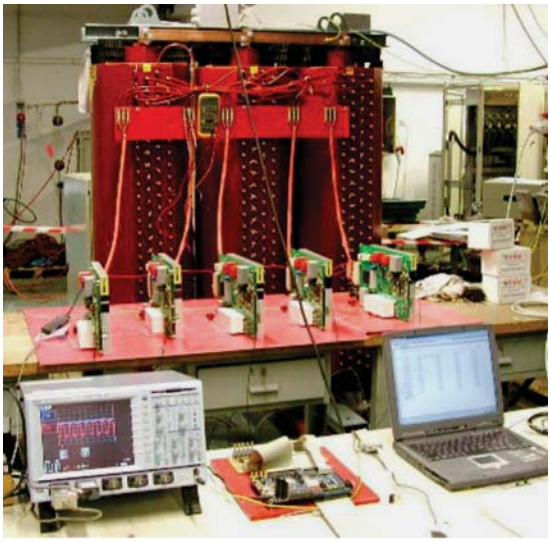

Fig. 3.14 - Testing of first ITER CDP gyrotron body power-supply modules with the related transformer

3.5.1 Remote handling maintenance

The remote handling group at ENEA Brasimone was involved in the ongoing activities concerning refurbishment of the divertor cassette mockup of the ITER reactor and remote maintenance of the IFMIF target system at the divertor refurbishment platform (DRP) facility. Work in 2004 was related to upgrading the systems for the facility and to performing a reliability assessment of the IFMIF replaceable back-plate bayonet concept prototype.

Upgrading of the DRP facility. Since delivery of the new ITER divertor cassette mockup, the DRP facility has undergone substantial upgrading of its major areas and systems: for example, separation of the hot-cell simulation and operator areas by a number of large portable screens, installation of a window to enable the operator to see inside the hot-cell area, installation of a new dual light manipulator station for the far side of the hot-cell simulation area, improvement of the viewing system (both hardware and software) and data acquisition system, installation of a safety system to enable workers and visitors to move about in a safe working environment, installation of the plasma-facing component transporter (PFCT). Figure 3.15 shows the layout of the hot-cell simulation area of the DRP facility. With the final architecture of the DRP facility, refurbishment operations can be carried out both for the cassette prototype and for the IFMIF target system.

Plasma-facing component transporter. The refurbishment operations of the new ITER divertor cassette mockup include remote attachment/detachment of the plasma-facing components (PFCs) - or “targets”. The cassette design was substantially changed (i.e., shape, weight and so on) after the review of the ITER project, which means that the devices and tools

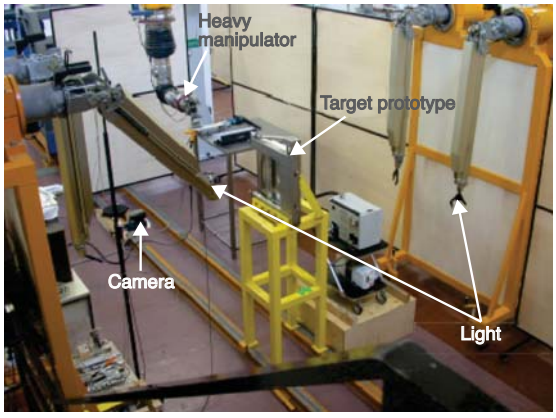

Fig. 3.15 - General view of the DRP hot-cell simulation area

required as well as the refurbishment procedures might have to be modified and, in some cases, completely redesigned. To carry out the refurbishment operations, a new device, the plasma-facing component transporter (PFCT), was mechanically designed and fabricated by the Italian firm of Ing. Candotti Impianti Industriali, Gorizia, installed and successfully tested by the end of July 2004. (fig. 3.16). The hardware and software control systems were designed and assembled by ENEA. The commissioning tests of the entire system were started in December 2004, and completion is expected by the end of February 2005.

Fig. 3.16 - General view of the PFCT

Development and modification of the tools. This activity began after the arrival of the new cassette mockup, but has proved to be much more complex than originally planned. The new cassette mockup requires general installation and removal of the three targets from both sides of the cassette. Furthermore, the pin for the multilink systems has to be disassembled by pulling rather than pushing, which means that the tools for the refurbishment cycle of the cassette mockup have to be modified or new ones developed. Some of the tools (new frame for drilling the pin; new and a modified version of the pin-extraction tool; new lifting frame for the inner vertical target) were delivered in December 2004 by Gradel S.A. of Luxemburg, who are manufacturing/modifying the tools under ENEA's supervision, and the remainder is expected at the end of February. The fabrication of a second new cassette mockup (fig. 3.17), especially equipped for thermal-hydraulic testing, has been planned. Assembly of this new cassette will require water-tight welds on all the cooling pipes, qualification of the welding process, design of appropriate procedures and procurement of suitable welding equipment. In June 2004 under an EFDA agreement ENEA was assigned the task of qualifying the process to be used for welding the PFC cooling pipes to the cassette body manifolds. Following a preliminary study, an internal automatic orbital tungsten inert gas welding process was selected by ENEA. During welding the pipe remains stationary, while the welding torch automatically rotates around the joint. A specific tender to select an industry with expertise in this field will be launched early in 2005.

Alternative methods for multilink pin extraction. The refurbishment trials executed during the last test campaign on the divertor cassette mockup, while demonstrating the feasibility of the assembly operations

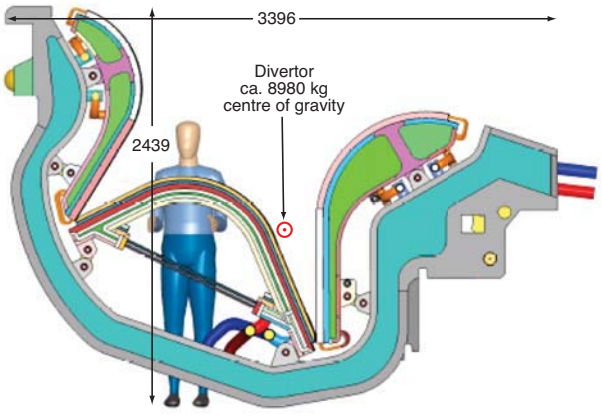

Fig. 3.17 - Model of the second new cassette prototype

References

[3.13] J-P. Hogge et al., *Development of a 2 MW, CW, 170 GHz coaxial cavity gyrotron for ITER*, presented at the 13th Joint Workshop on ECRH (Nizhny Novgorod 2004)

also indicated that the dismantling operations needed improvement in terms of the effectiveness and reliability of the process used to extract the pins. The process was initially based on a drilling tool that removed the stressed material in the centre of the pin, causing the remaining outer part to collapse and enabling its extraction by simply pushing it out. This dismantling process had various problems, including breakage of the drill bit, damage to the multilink blocks and damage to the pin itself. To improve this kind of extraction process, several potential alternative methods to extract the pins from the multilink attachment systems were investigated. The investigation was based on the following premises: the pin should be exactly the same as that used in the previous multilink trials (i.e., material already fixed and identical pin dimensions); the assembly process should be executed by means of the existing expanding tool; the pin disassembly process should not produce swarf. Three thermo-mechanical methods were proposed: a cooling method based on rapid cooling of the pin by means of a cryogenic cylinder; a heating method, changing the dimensions of the materials by high-temperature heating only; a mixed method based on a combination of both cooling and heating. ANSYS simulation of the processes demonstrated that the mixed method would be the most suitable for pin extraction, and the tool proposed for this operation appears to be feasible. The work was carried out in collaboration with the University of Pisa.

3.5.2 Viewing and ranging systems for ITER

During 2004 the activities in collaboration with the ENEA Applied Physics Technologies Unit (for the electro-optics) were mainly devoted to deeper experimental analyses of the probe performance [3.14,3.15] and those in collaboration with CEA to identifying the target (first wall and divertor) area that can be scanned with the presently foreseen number of probes, i.e., np=6. In fact, the submillimetric viewing and ranging (i.e., 3D images built by merging target ranging and viewing data) performance of the system depends both on the target distance (2–10 m) and on the beam incident angle ($\leq 60°$) on the target. While the first parameter can be managed by installing an autofocus device on the probe launching optics, the beam incident angle depends on the number and position of the probes. Studies show that in the present situation not more than 75% of the first wall and less than 50% of the divertor zone can be efficiently scanned. Hence, experimental characterisation of the probe on typical ITER in-vessel components has been planned for 2005.

A special version of the in-vessel viewing and ranging system (IVVS) probe for use inside hardly accessible archaeological zones has been developed and built outside the ITER programme. Its experimental testing is expected during the second half of 2005.

3.6.1 Design of ITER neutron camera

A detailed design analysis for the ITER neutron radial camera (EFDA contracts 02-1002 and FU06/CT 2003-00020) was performed [see ref. 1.73] by means of the MCNP code and a general model that was modified to include the radial camera system in one of the equatorial ports as well as to describe both the ex-vessel (12×3 lines of sight) and in-vessel (9 lines of sight) detecting systems. The aim was to determine the expected neutron/gamma-ray fluxes and spectra at the detectors and, more in general, to assess the performance of the diagnostic. The effect of the camera movements relative to the machine was also investigated. Neutron fluxes/spectra as well as photon fluxes/spectra were determined in different regions where detectors are supposed to be placed (for the ex- and in-vessel systems). The neutron spectra provided by MCNP calculations indicate that for the ex-vessel lines of sight the scattered neutrons are about a fraction of 0.1% of the 14-MeV neutrons for the 1-cm-diam collimator and about 0.4% for the 2–cm-diam collimator. The scattered neutron contribution for the in-vessel lines of sight is higher (in the range 1-5%). Cross-talk and backscattering were also studied. Neutron fluxes at the detectors were cross checked with analytical calculations. Response variations to the reciprocal movements of the in-vessel components and the radial camera were also investigated.

3.6.2 Experimental validation of neutron cross sections for fusion-relevant materials

Neutronics experiment on a TBM–HCPB mockup. A neutronics experiment is to be performed on a mockup of the test blanket module (TBM)-HCPB concept at the 14–MeV Frascati neutron generator (Task TTMN-002 –D2) [3.16]. The experiment will be conducted in 2005 and will be followed by a second experiment on a HCLL mockup. The purpose of the experiments is to validate the codes and nuclear data used in the design of TBMs and later in the breeder blanket for fusion reactors. They will include the measurement of the tritium production rate in the breeder material and the neutron/gamma-ray fluxes and spectra in and behind the mockup. The experimental results will be compared with the numerical predictions.

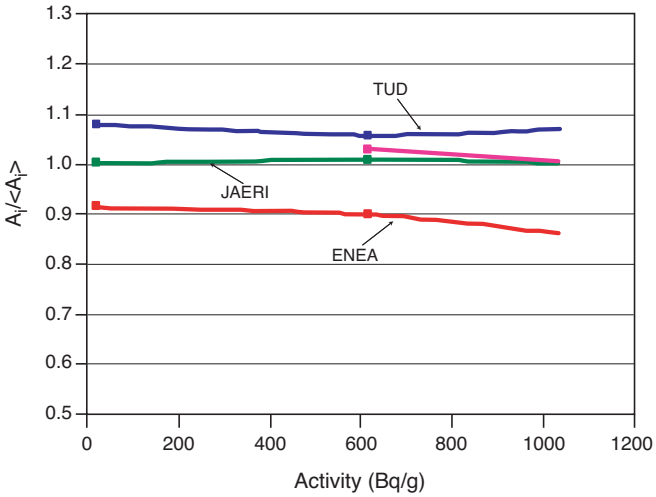

Fig. 3.18 - Tritium activities A_i measured in different laboratories in Li_2CO_3 pellets irradiated with 14-MeV neutrons, normalised to the mean of the measured activities $<A_i>$

During 2004, the mockup of the TBM-HCPB was built according to the previously agreed design. The steel components (container, tubes and the capsule used for the detectors) and breeder cassettes (filled with Li_2CO_3 powder) were built by ENEA. The mockup was then filled with metallic beryllium at the Bochvar Institute of Inorganic Materials (VNIINM) of Moscow, Russia. While the mockup was being constructed, tritium measurements and calibration techniques were inter-compared between ENEA, the Technical University of Dresden (TUD) and JAERI, using Li_2CO_3 pellets irradiated with 14-MeV neutrons [3.17]. The intercomparison of measurements obtained in the three laboratories on equivalent samples showed a relative standard deviation of about 7-8% (fig. 3.18). The three laboratories will participate in the TBM-HCPB mockup experiment in 2005.

Validation of activation cross sections of tantalum. Tantalum is found in materials such as EUROFER and in the brazing alloys used in a fusion reactor. Pure samples of tantalum were irradiated with 14-MeV neutrons at FNG to compare the activation characteristics of the material with the prediction of the inventory code EASY-2003 (task TTMN-002-D8). The neutron-induced decay heat in the irradiated samples in a first-wall-like neutron spectrum was measured.

Two tantalum samples were irradiated for about four hours. One sample was monitored by the ENEA decay-heat measuring system, which simultaneously measures gamma and beta decay heat. The other sample was monitored by high-purity germanium detectors. The decay times studied ranged from a few minutes up to some days after irradiation. Experimental data and EASY predictions for both beta and gamma rays compare quite satisfactorily for all the measured decay-time intervals (fig. 3.19). With gamma spectroscopy it was possible to identify the radionuclides produced by neutrons and hence the nuclear reactions that mainly contribute to the induced activation. One of these nuclear reactions, predicted by EASY, had never been validated by experimental measurements. Seven reactions were identified

References

[3.14] C. Neri et al., *Experimental result of the laser in vessel viewing and ranging system (IVVS) for ITER,* presented at the 23rd Symp. on Fusion Technology – SOFT23 (Venice 2004)

[3.15] C. Neri et al., *Parallel hardware implementation of RADAR electronics equipment for a LASER inspection system*, presented at the IEEE Nuclear Science Symposium, (Rome 2004)

[3.16] U. Fischer et al., *EU blanket design activities and neutronics support efforts,* submitted to Fusion Science and Technology

[3.17] P. Batistoni et al., *International comparison of measuring techniques of tritium production for fusion neutronics experiments - status and preliminary results*, presented at the 23rd Symp. on Fusion Technology – SOFT23 (Venice 2004)

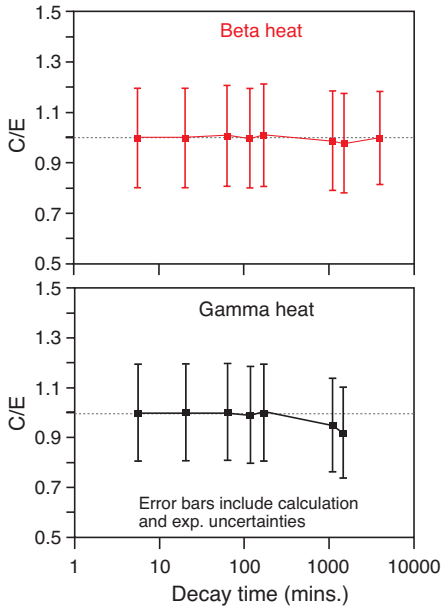

Fig. 3.19 - Results from decay heat measurements for beta and gamma heat

as being responsible for more than 99% of the heat produced in the measured decay time and can be used to validate the European Activation File (EAF) database.

3.6.3 Development of single-crystal CVD diamonds for radiation detection

It has been shown that synthetic diamond is a suitable material for both radiation and high-energy-particle detectors. Radiation-hard diamond-based neutron detectors have been developed under a collaboration between ENEA and the Department of Mechanical Engineering of Rome Tor Vergata University and are being tested in JET for prospective applications in ITER. The collaboration has led to Tor Vergata becoming an associate in the Euratom project on fusion.

The most widely used technique to produce artificial diamond films is probably chemical vapour deposition (CVD) because of its high reliability. However, the polycrystalline nature of heteroepitaxial CVD samples constitutes a severe limitation on the device performance in any field in which good electronic properties are mandatory. This is why a great effort is now being devoted in many laboratories to the growth both of synthetic single-crystal diamond and of homoepitaxial diamond films.

Homoepitaxial diamond films were deposited in a modified microwave plasma CVD tubular reactor on a low-cost synthetic high-pressure high-temperature (HPHT) single-crystal diamond substrate. The CVD diamond layers were deposited at 700°C in a 1% CH_4/H_2 mixture with a 1.2 μm/h growth rate. The lattice parameter was estimated by SEM and XRD analysis to be 3.571 Å. A detector prototype was built up from such a diamond film by evaporating metallic contacts in a sandwich geometry, without removing the HPHT 315-mm-thick substrate. Both circular Au and Al were tested as 2-mm-diam, ~100-nm-thick metallic contacts. The sample was placed in an Al housing, so that irradiation on both the growth and the substrate side was possible. Figure 3.20 reports the response to the triple Pu-Am-Cm alpha source in the case of a +80 V bias polarity, i.e., with +80 V on the CVD diamond growth surface. A full width at half maximum

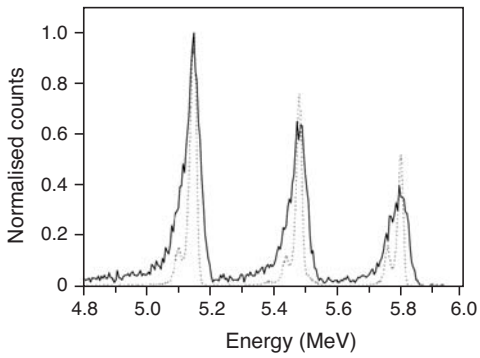

Fig. 3.20 - Comparison between Si and diamond detector response to the triple 239Pu 241Am 244Cm alpha source. The vertical scale was normalised to the 239Pu alpha peak intensity, while the energy axis was scaled up to superimpose the alpha spectra from the two devices

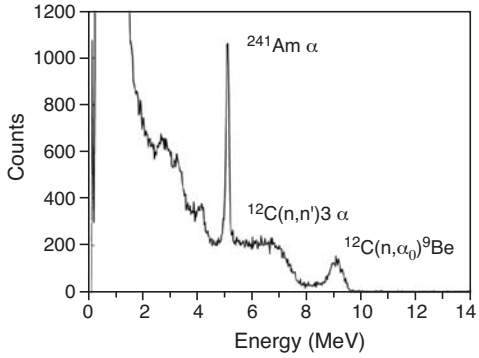

Fig. 3.21 - Neutron spectrum from 80-V positively biased diamond detector irradiated with 14.8-MeV neutrons at FNG. A 0° detector angular position vs. the deuteron beam was adopted. Alpha irradiation by a 241-Am source, 4.2 mm from the detector surface, was simultaneously performed to allow a straightforward energy scale calibration

(FWHM) better than 1% was measured. The detector was thus exposed to 14-MeV neutrons at FNG and the pulse height spectrum was recorded. The peak due to the $^{12}C(n,a_0)^9Be$ reaction, produced by the 14–MeV neutrons (reaction threshold >6 MeV) is clear (fig. 3.21). The energy resolution (FWHM) is <3% and is directly comparable to the best performance of natural diamond detectors as well as of other single-crystal diamond detectors. The detector has been proposed as a 14-MeV neutron spectrometer at JET for the 2005 campaign.

3.7.1 SiC/SiC composite development

The activity concerning the use of SiC/SiC ceramic composites for plasma-facing components is aimed at manufacturing SiC_f/SiC composites with advanced fibres and improved interphase and matrix by the isothermal chemical vapour infiltration (CVI) technique. Under a collaboration between ENEA and FN–Nuove Tecnologie e Servizi Avanzati SpA Italy, a medium-size facility (fig. 3.22) allowing both CVI and CVD processes was built and installed at FN in 2004. The facility is intended as a flexible tool for investigating alternative infiltration processes and manufacturing small samples or medium-scale mockups with a half-finished shape (tubes or boxes). The volume available for processing is a 300-mm-diam, 400-mm-high cylinder accessible from the top of the reactor. Small samples (e.g., flat tiles), tubes or half-finished shape preforms can be infiltrated. The total power of the facility is 25 kW, and the maximum reachable temperature in the reactor is 1400°C. The resistors are housed in a double-shell AISI 304 stainless steel vessel actively cooled by water. The maximum vacuum obtainable is 0.5 mbar with no gas and 10 mbar during the process. The gas duct system includes CH_4 (for C interphase deposition on fibres), metil-thrichloro-silane as SiC precursor, N_2 and Ar as purge gas and H_2 as carrier. Filters and a Venturi-scrubber system are used for gas purification. The process can be monitored by means of a remote control panel which is computer-assisted for data recording. A final check of the facility was completed successfully.

Fig. 3.22 - CVI/CVD facility

Preliminary cyclic testing was performed to investigate the fatigue behaviour of Cerasep N4-1 commercial grade SNECMA [3.18]. Flexural cyclic tests were done at room temperature (RT) and at 1000°C; a sinusoidal wave form stress amplitude was used with a frequency of 1 Hz. The peak stress (σ_{MAX}) imposed for testing varied from 50 MPa to 80, 100 MPa, but tests with higher s_{MAX} were also carried out stepwise up to 290 MPa. A minimum stress (σ_{MIN}) of 20 or 50 MPa (depending on the σ_{MAX} value) was imposed in order to keep the specimen in place in the bending test fixture. Early studies on the fatigue of ceramic matrix composites support the observation that the fatigue stress threshold is below the threshold at which crack growth occurs. In the present case preliminary tests at RT suggest that the stress threshold is lower than the matrix cracking stress. The composite investigated is able to withstand peak stresses of 50 and 80 MPa for more than 10000 cycles, but 100 MPa can be withstood for about 1000 cycles. The number of cycles to failure is sensibly reduced with testing at 1000°C. In this case a peak stress of 80 MPa can be withstood for about 1000 cycles (10000 cycles with 50 MPa peak stress). Cyclic stress-strain curves showed no degradation of the hysteresis loop with low peak stress (sufficient to allow the material to withstand 10000 cycles, i.e.,

References

[3.18] B. Riccardi et al., *Mechanical characterisation of commercial grade SiC_f/SiC composites*, Proc. of 6th IEA Workshop on SiC_f/SiC Composite for Fusion Reactors (Boston 2004), in press

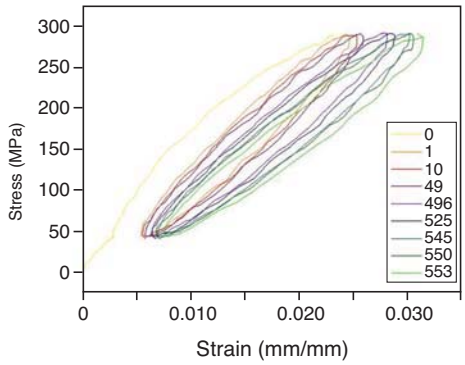

Fig. 3.23 - Bending cycles under high peak stress at RT (290 MPa)

up to 80 MPa at RT and 50 MPa at 1000°C) but sensible changes in the loop when the peak stress is higher (fig. 3.23).

Preliminary stress rupture testing was performed to investigate the creep behaviour of Cerasep N4-1. Four-point bending tests were carried out using the same specimen size as in the cyclic tests. As-received Si-coated specimens were used to evaluate the effect of the testing atmosphere. The testing temperature was 1000°C, the applied bending stress 100 Mpa and the test atmosphere was an argon gas flow (20 l/h) with renewal five times/hour in the furnace. The thermal cycle consisted of heating to 1000°C, 4.5°C/min, 40-min hold time, load application, testing and natural cooling (with flowing gas). The outcome of the tests is that the creep resistance of the material investigated appears rather poor at the stress value used (100 MPa). Due to the matrix cracks after load application, the crack bridging fibres are directly exposed to the environment. The time to rupture ranged from 16 to 143 h. No substantial difference in results was found between as-received and Si-coated specimens. The failure was almost brittle with pullout nearly zero and no detachment of the fabric layers. Figure 3.24 shows a typical strain vs. time curve (total and creep strain).

The molecular dynamics simulations of radiation damage in crystalline cubic SiC were continued. The reliability of the CAST code was assessed by incorporating a special version of the Tersoff potential. The CAST code was improved for low-energy recoil simulations by performing selected molecular dynamics experiments at very low energies (of the order of 20-50 eV PKA for both Si and C primaries) and well controlled streaming directions in the crystal lattice. The results of the simulations were compared with other published data. The short-range part of the interaction potential was characterised. In a first implementation of the code the range of the simulations was extended up to 2 keV PKA at 300K for both Si and C primaries. In such conditions an almost linear increase of permanent damage with increasing primary energy was found. A somewhat pronounced preference for defect cascade creation was observed in the case of C primaries. By comparing the initial damage with the cascade distribution after equilibration, no major differences were found between Si and C primaries in the range 0.25-2 keV. In general C interstitials were the prevalent type of defect over the whole range of energies explored, but at energies higher than 1 keV, a sizeable fraction of substitutional defects (antisize) was observed.

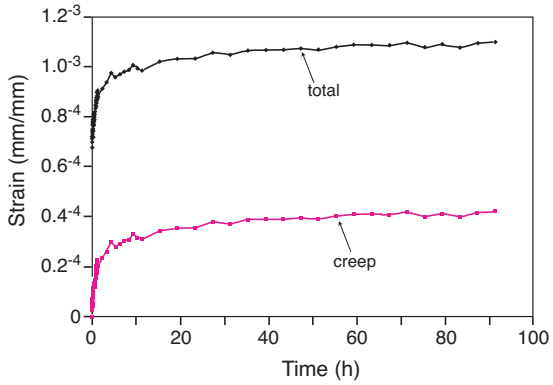

Fig. 3.24 - Total strain and creep strain vs. time

3.7.2 Reduced-activation steels

The work on characterising improved EUROFER welds (CEA-made) relative to fatigue or impact resistance continued. Data on the effect of post-welding heat treatment (PWHT) on the mechanical properties and structural features of gas-tungsten arc-welded (GTAW)+filler material joints are available. Properties such as tensile and impact strength were studied on welded plates heat treated at 730 and 750°C for a soaking time of 1 and 2 h. Although the short-term properties of the welded joints seem to be acceptable, the results from creep and fatigue tests were unsatisfactory. Stress-rupture creep tests were carried out at

500°C on base material and EBW joints, “as welded” and PWH treated. At high stress (280 MPa) the times to rupture of the joints are fairly similar; at medium stress (250 MPa) and at the lowest stress level (220 MPa) a significant loss of strength was observed for the PWHT samples.

Low-cycle fatigue (LCF) tests on EBW joints were performed by using a load-control method and, to shorten the test duration, an extremely severe loading condition was used. The test parameters were a temperature of 450°C, a maximum load corresponding to 435 MPa and a minimum load of 43.5 MPa (R=0.1). Although the base material showed a fatigue-life of about 1×10^5 cycles under the same test conditions, the joint treated at 730°C for 1 h failed after 4692 cycles, and the joint treated at 750°C, at 382 cycles. Long-term properties seem seriously affected, due perhaps to precipitation or to segregation phenomena occurring during the PWHT.

The physical-mechanical properties of EUROFER steel, the thermal expansion coefficient (CTE) and Young’s modulus as a function of temperature were investigated. The CTE was measured under static and dynamic thermal conditions. The results showed that there is no relevant difference between EUROFER and F82H alloys. The tests were carried out in the range 20-700°C.

The impact properties of the CEA-manufactured EUROFER oxide dispersion strengthened (ODS) were studied from 300°C to –300°C. The specimen orientation seems to have no influence on absorbed energies. Therefore, it can be said that no texture is present in the 6-mm-thick plate tested; the material appears homogeneous. The longitudinally and transversally oriented DN 50 115 Kleinstprobe standard specimens showed a ductile-to-brittle transition temperature (DBTT) close to 10-12°C, which is a good improvement on the 90-100°C estimated for the previous ODS generation. Unfortunately, these good characteristics are zeroed by the absorbed-energy values. In the upper shelf energy field, a mean value of 2.33 J was measured at a temperature over 60°C. Fracture toughness, although roughly estimated, showed very low values.

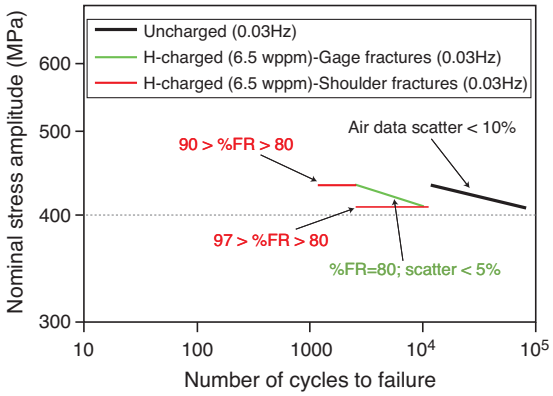

Fig. 3.25 - LCF curves of EUROFER 97 TGA weldment

Hydrogen degradation effects on the mechanical properties of EUROFER 97 base metal and GTAW joints were investigated by means of fully-reversed load-control LCF testing at room temperature and under cathodic charging on specimens pre-saturated with hydrogen. Two electrochemical conditions were selected for base steel, which provided hydrogen contents at around 2-2.5 wppm and 6-6.9 wppm. Increasing the hydrogen supply caused the material to become increasingly receptive to damage, but enlarged the data scatter in terms of fatigue lifetimes and cracking modes, especially at lower frequency. Specimen fracture was fully ductile in the uncharged condition, but varied from intergranular to transgranular as internal hydrogen was increased. Microscopic inspection suggested that the damaging mechanisms for steel in the normalised and tempered state probably involve hydrogen-induced plastic flaw blocking and interface de-cohesion. There was also some fractographic evidence supporting the inference that the EUROFER microstructure is inhomogeneous [3.19]. Low cycle fatigue failure of the uncharged EUROFER welded joint (fig. 3.25) always occurred in the heat affected zone. The corresponding fatigue lives were longer than those of base

References

[3.19] M.F. Maday, G. Filacchioni and L. Pilloni, *A comparative study about the hydrogen embrittlement suceptibility of Eurofer'97 and conventional 9%Cr ferritic/martensitic steels,* Proc. of the 20th IEEE/NPSS Symposium of Fusion Engineering (San Diego 2003) pp 185-188

steel and were variably impaired by hydrogenation under the most severe condition (6–6.9 wppm). Premature fracture through tests on hydrogenated samples occurred either in the hard molten zone (by brittle microcleavage) with reproducible cycles to failure, or within the soft overaged region of the heat-affected zone (by brittle fracture through trans-granular shearing starting from coarsened carbides) with scattered lifetime reduction.

Post-irradiation small-angle neutron scattering (SANS) inspection of irradiated RAFM steels continued. The final SANS data on 2.5 dpa EUROFER were presented at the SOFT23 Conference in collaboration with FZK and the Energy Research Foundation (ECN) Petten [3.20]. A new SANS experiment on several 9–15 dpa neutron-irradiated EUROFER 97 samples to be provided by FZK has been prepared at the High Flux Reactor of the Institute Laue Langevin (ILL) Grenoble. Delivery of the irradiated material has been delayed, but the experiment should be carried out in March 2005. Unirradiated reference samples will be tested as well. Unirradiated EUROFER ODS material will also be studied to continue the microstructural investigation of different metallurgical treatments.

3.8.1 Lithium corrosion and chemistry

The LIFUS III loop for testing cold and hot traps, non-metallic monitoring devices and evaluating the corrosion/erosion rate in IFMIF representative conditions is being characterised by means of water (task TTMI-002-D4). The most promising techniques for the non-metallic control and monitoring systems were selected by ENEA and the University of Nottingham, and suitable sensors and traps to be installed in the loop have been designed. Some offline analytical techniques for detecting dissolved impurities have been tested, i.e., capillary specific resistivity measurements for nitrogen, the equilibrium foil method for other impurities. The preliminary experimental results are under analysis.

3.8.2 Lithium target replaceable back-plate

Cavitation tests at the electro-magnetic pump and at the joint of the replaceable black-plate. The occurrence of cavitation was tested at Osaka University lithium facility from 19-23 April 2004 (task TTMI-002-D2). Two ENEA CASBA-2000 accelero-meters were screwed onto the loop close to the inlet of the electromagnetic pump (EMP) and at the outlet of the flow straightener. A dedicated data acquisition system on a PC notebook and LabView software were prepared by ENEA and linked to the loop control process system in the control room. The loop hydraulic performance at the nominal lithium temperature of 310°C was calculated on the basis of the available data of the EMP, piping geometry and experimental measurements. During the tests the argon pressure in the gas separator at

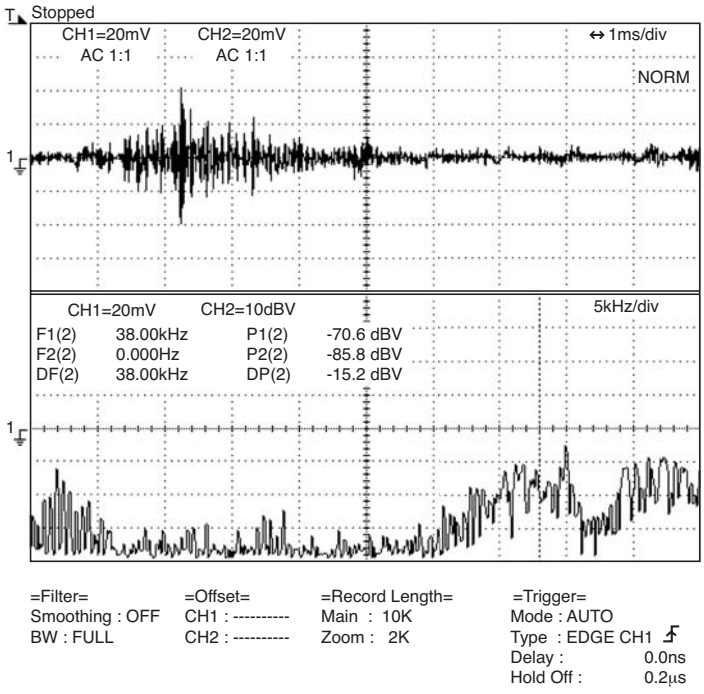

Fig. 3.26 - Cavitation at EMP inlet (nozzle velocity 13.3 m/s and argon pressure 0.065 MPa)

the outlet of the nozzle was kept constant, while increasing stepwise the EMP flow rate. Five different flow-rate ramps were performed at absolute argon pressures of 0.05, 0,065, 0.09, 0.11 and 0.135 MPa. During the whole test campaign, the temperature of the lithium inlet to the EMP was kept at about 305-310°C. The first detection of cavitation noise was recorded by CASBA 2000 close to the EMP inlet at an argon pressure of 0.05 MPa and a nozzle velocity of 12 m/s; the second was recorded at 0.065 MPa and 13.3 m/s (fig. 3.26) and the third at 0.09 MPa at 15 m/s. In all three cases, some acoustic noise was also heard during cavitation. The magnitude of the CASBA 2000 response and its signal amplification are evident both in dB and in the linear plot of the root-mean-square signal, DC-out. No cavitation was recorded at the EMP inlet at an argon pressure of 0.11 MPa up to the maximum permissible nozzle velocity of 15 m/s. No cavitation signal was detected at the flow straightener-orificed plates upstream of the nozzle up to 15 m/s of lithium flow velocity with argon absolute pressure higher than 0.05 MPa.

Water experiments at the joint of the replaceable back-plate. Additional water jet experiments on the IFMIF simulated target system were started at the end of 2004 at the CEF 1-2 thermal hydraulic facility at ENEA Brasimone (task TTMI-002-D3). The hydraulic tests were performed on the HY-JET mockup simulating the IFMIF lithium jet flow with a double reduced nozzle on a curved target back-plate of curvature 250 mm and surface roughness 1 mm. The tests on the hydraulic characterisation and the flow instabilities close to the nozzle-backwall zone were repeated (fig. 3.27).

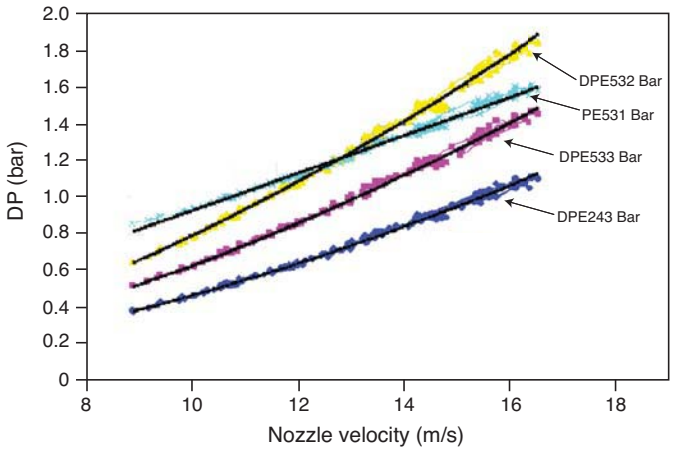

Fig. 3.27 - Hydraulic characteristics of the flow straightener and orificed plates (back-plate curvature 250 mm, T = 55°C)

Reliability assessment of the replaceable back-plate. The remote handling (RH), vacuum and leak-rate requirements for the removable back-plate (bayonet concept) were assessed. In 2004 a reliability test campaign on the RH procedure was carried out, completing 100 RH cycles including 50 mounting and 50 removal procedures (fig. 3.28). The reliability trials confirmed the main results already obtained in the 2003 campaign: the prototype is well suited to remote handling (i.e., back-plate replacement operations were completed successfully each time) and the repeatability replacement time is less than two days. The replacement time was reduced after improving the prototype characteristics and modifying the procedure (back-plate replacement is currently carried out using only one tool); in general

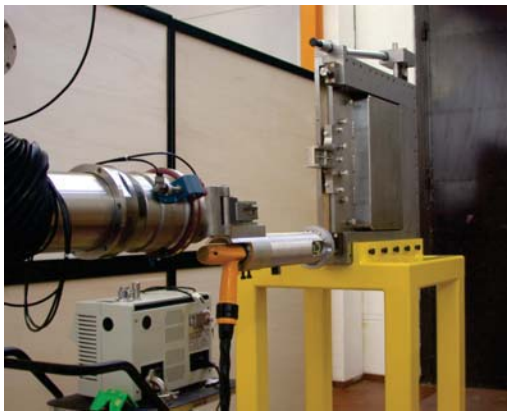

Fig. 3.28 - IFMIF lithium target back-plate reliability test

References

[3.20] R. Coppola et al., *Microstructural investigation, using SANS, of neutron irradiated Eurofer97 steel*, Presented at the 23rd Symp. on Fusion Technology - SOFT23 (Venice 2004)

the prototype did not suffer significant damage; the vacuum test confirmed the results obtained during the test campaigns; the back-plate positioning repeatability was within ±0.1 mm from the average back-plate position.

The rescue procedures to assess the behaviour of the prototype under possible failure conditions are under development. The procedures for the failure conditions identified are based on the results of the reliability assessment and on the experience gained during the previous tests. A set of tools for performing the rescue procedures has been selected.

3.8.3 Safety analysis

The activity had two objectives: identification of a set of reference accident sequences [3.21] involving the whole IFMIF plant and deterministic assessment of a couple of the sequences [3.22]. The study identified qualitatively the most significant accident sequences that could potentially occur during normal operation and possibly constitute a public and environmental hazard. The accident sequences were developed starting from selected initiators and then defining sequence families (or plant damage states). The initiating events considered were based on similarities in plant response and accident evolution. Then for each sequence family, reference sequences were selected as being considered the most challenging from the safety viewpoint. The "credibility" of these sequences should be supported by a probabilistic quantification analysis, which would exclude the sequences having a negligible likelihood of occurrence. Deterministic analyses will be required to evaluate the potential of the reference accident sequences to impair the integrity of safety barriers (e.g., containment) and cause the release of radioactive material. The accident analyses considered two sequences involving the lithium target and accelerator-beam cooling loop. The aim was to verify whether in out-of-normal conditions the integrity of the components be compromised and there exist the risk of radiological release. The first accident hypothesized was a 10% overpower for 20 s in one of the beams because of over-voltage or over-current. The beams of today's accelerators are not entirely stable, so it is necessary to know what effects their behaviour has on the thermal structures of the lithium target (thermal shocks) and on the cooling in the pipes. This type of accident initiator is unique to accelerator-driven systems and the phenomena behind it are still an open question. Although the probability that this kind of accident occur is extremely low as there are numerous control systems, its analysis is important in the design of a safe facility. The consequences identified are a very limited increase in the temperature of structures and coolant, which has no effect on fluid pressure because of the short duration of the anomalous transient. The second accident analysed was water leaking from the beam cooling loop, entering the beam duct and breaking the vacuum conditions. Because of the low water-temperature, a very limited amount of vapour is generated due to flashing in the vacuum environment. Nevertheless, spray from the jet of water can cause droplet atomization, and some vapour can come into contact with the lithium flowing in the target zone when the fast-isolation valves fail. The reaction between vapour and lithium generates heat and hydrogen. Analyses showed that although the hydrogen in the total beam volume is not sufficient to detonate or deflagrate, it can constitute a risk if it becomes concentrated in zones and oxygen enters the beam duct.

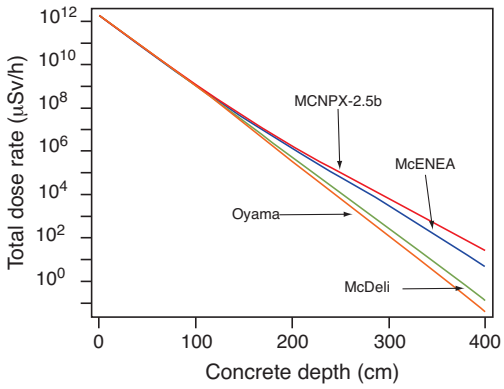

Fig. 3.29 - Comparison between total dose rates obtained with different neutron sources in heavy concrete

Assessment of the impact of the neutron source on dose rates outside the test cell shielding walls continued. A new neutron source model, McEnea, was developed according to the measurements of neutron emission spectra in Li(d,n) reactions for 40-MeV deuterons performed at the Cyclotron and Radioisotope Centre

(CYRIC), Tohoku University, Japan. Full 3D neutron transport calculations were performed by MCNP codes to obtain the dose rates outside the test cell shielding walls and in the access/maintenance room. The reference shielding material of the test cell walls was assumed to be heavy concrete. The results obtained with McEnea were compared (fig. 3.29) with those obtained using other available neutron sources, i.e., Oyama, McDeli and the MCNPX 2.5b internal model. It was found that high-energy neutrons (>40 MeV) are significant (90% of the total dose) in evaluating the shielding. The Oyama and McDeli models do not take into account the neutrons produced in exothermic D-Li reactions, so they are not suitable for application in IFMIF dose rate calculations (148 μSv/h and 320 μSv/h respectively for 300 cm). The MCNPX-2.5b internal model uses a statistical model which is not correct for light nuclei and unrealistically predicts neutron energies up to 80 MeV (7496 μSv/h for 300 cm). According to the new McEnea model, based on recent experimental data, the thickness (400 cm) of the heavy-concrete shielding front wall is sufficient to meet the requirements of the maximum allowable limit of 10 μSv/h in the operative areas of the IFMIF facility (3281 μSv/h for 300 cm and 5 μSv/h for 400 cm).

3.8.4 Cost assessment of conventional facilities

The cost assessment review of the IFMIF conventional facilities took into account the design development reported in the IFMIF Comprehensive Design Report (December 2003). The assessment considered the main building complex, administration building and other service buildings; heating, ventilation and air conditioning (HVAC) system; central control and common instrumentation (CC & CI) system [3.23].

The main building complex was divided into i) the bunker building, which is a basement consisting of shielded areas and cells and ii) the industrial building and the rest. The building cost was estimated by a bottom-up procedure based on prices quoted in the Italian civil engineering manuals published in 2004. The overall estimate, including cranes, stack and site preparation is 51,211 k€. Comparison with the estimate reported in the IFMIF Cost Estimate, Appendix F, is quite good, with only a +0.03% difference in the overall cost, although some items (i.e., cranes, stack and administration and service buildings) show a larger difference.

The cost of the HVAC system cost was assessed dividing the system into i) the industrial HVAC and ii) nuclear HVAC, which in turn was divided into three subsystems (nuclear HVAC, nuclear HVAC plus emergency detritiation, and nuclear HVAC treating argon gas). The results of the assessment were industrial HVAC system ~ 1135 k€ and nuclear HVAC system 14,751 k€, for an overall cost of ~15,886 k€.

The cost of the CC & CI system was estimated to be 11,349 k€.

3.9 Safety and Environment, Power Plant Studies and Socio-Economics

3.9.1 Collection and assessment of JET occupational-radiation data

The 2003 analysis of annual worker doses was repeated with the additional data obtained from JET, and a new analysis based on the monthly dose information from JET was also carried out [3.24].

References

[3.21] R. Caporali, L. Burgazzi and T. Pinna, *Definition of reference accident sequences for IFMIF safety assessment*, ENEA Internal Report FUS-TN SA-SE-R-107 (2004)

[3.22] R. Ferri and M.T. Porfiri, *IFMIF accidental sequence simulation on the lithium loop and accelerator by RELAP5 and CONSEN codes*, ENEA Internal Report FUS-TN SA-SE-R-104 (2004)

[3.23] L. Di Pace, *Cost assessment of IFMIF conventional facilities, central control and common instrumentation – intermediate report*, ENEA Internal Report FUS-TN-SA-SE-R-111/Rev. 1, (2004)

[3.24] A. Natalizio and M.T. Porfiri, *Radiation exposure analysis – data relating to the years 1988-2003*, ENEA Internal Report FUS-TN SA-SE-R-118 (2004)

Two empirical dose correlations for the pre-ALARP (as low as reasonably possible) period and two for the ALARP period were obtained. For the pre-ALARP period CD=0.975 SDT, CD=0.0221 NP T, while for the ALARP period CD=0.185 SDT, CD=0.0323 NP T, where CD is the collective dose, SDT the shutdown time in days, NP the number of monitored people and T the exposure time. Although there is a level of uncertainty associated with the analysis results, the above correlations demonstrate a significant improvement in machine operation from a radiation protection perspective, after the introduction of the ALARP policy. The monthly data enabled a more detailed analysis of JET radiation exposure experience. The analysis was focussed on work effort, as this is the most difficult parameter to determine when estimating future doses for either JET or ITER. Despite the large uncertainty with respect to the work effort estimates, and despite the stochastic errors in the statistical analysis, results relying only on comparisons have a higher level of confidence. It can be concluded from the analysis that the introduction of the ALARP policy at JET had a significant positive impact on worker radiation exposure. A better understanding of the improved work practices resulting from the application of ALARP at JET would be of benefit to ITER as the JET experience will establish de facto benchmarks.

3.9.2 Collection of JET component-failure data

A collection of fusion-specific data relative to JET component failures was built up [3.25]. The work concerning the vacuum and active gas handling systems [3.26] was extended in 2004 to the JET neutral beam injectors (NBIs) and power supply systems. The overall set of available information related to out-of-normal operating experience at JET was retrieved and collected in spread sheets of "data events". The components installed in the two systems were classified by type, number of installations, total operating hours and total number of operations on demand, as well as failure modes and causes. Failure rates with regard to operating days, pulse duration and failure probability on demand were estimated, where possible, and their mean values and uncertainty distributions calculated.

About 1935 records related to failures/malfunctions of the coil and NBI power supply and 90 failures related to NBI mechanical components were singled out. Statistical evaluations were performed for subsystems and main components, such as converters, flywheel generators, transformers, busbars, capacitors, inductors, resistors, circuit breakers, switchgears, vacuum switches, solid state devices, neutralizers, ion sources, etc. It should be noted that the present set of reliability data is one of the most consistent ever to be evaluated in the field of fusion facilities, both for the number of components and for the total operating hours dealt with. The calculated data will be very useful for evaluating reliability parameters in support of safety assessments and for availability/reliability analyses of fusion machines/plants. Statistical data obtained from "data events" will be recorded in the "Fusion Component Failure Rate Database".

3.9.3 Tritium diffusion

The objective of the experiments, performed at the Frascati STARDUST facility, is to investigate how tritium diffusion from the vacuum vessel (VV) to the vault can be counteracted if a connection is opened between the two volumes because of a loss-of-vacuum accident (LOVA) or a loss-of-coolant accident (LOCA). It is important to reduce tritium diffusion both to limit possible effects on operators and to allow for delayed intervention [3.27].

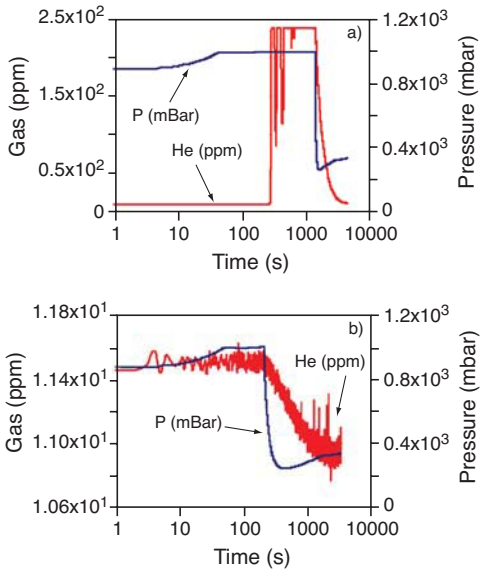

Fig. 3.30 - Helium migration from VV to vault (hot walls, 110°C)

Two types of tests were carried out: with cold walls (20°C) and with hot walls (110°C), at initial atmospheric pressure in the VV. The cold-condition test was aimed at demonstrating that the diffusion phenomenon is not so significant because the light gas (helium in the experiments, due to its affinity with tritium) is stratified in the upper parts of the VV and, in this case, its diffusion can be safely controlled even in the worst situation.

In all the tests a pipe break was used to simulate a leak at the equatorial level of the VV. The gas was pumped out by a dedicated pumping system to avoid its exit towards the vault. This setup demonstrated (fig. 3.30) that in hot conditions, if leakage does not occur in the vessel dome, the pumping system can stop the gas from diffusing in the volume simulating the vault. Therefore, an appropriate pumping system in the ITER VV could prevent tritium from escaping into the environment in the case of a LOVA, provided the pump can intervene soon enough after the break [3.28].

3.9.4 Analysis of selected ITER accident sequences

The objective of the analysis [3.29] was to identify the bounding accident sequences with the highest environmental impact, relative to the ITER tritium plant. The postulated initiating event - potential impact table (PIE-PIT) methodology was used. The potential consequences of each PIE were studied in detail to better understand the possible accident sequences related to tritium systems. The PIE-PIT pointed out the relationship between PIEs and plant confinement states (PCSs), which represent the plant conditions at the end of accident sequences. The PCSs were defined according to the source terms and the confinement barriers challenged during accident evolution. Each source term and each possible pathway through confinements were considered. Three bounding accident sequences were identified:

1. Break of a tritium process line inside the glove box (GB) of the storage and delivery system, aggravated by loss of GB confinement integrity and failure to isolate the nuclear HVAC system.
2. Break of isotopic separation system process line inside cold box (CB), loss of CB integrity, aggravated by failure to promptly isolate the HVAC.
3. Break of the water detritiation system blow-down tank in the operating room, aggravated by failure to promptly recover the pool generated in the room sump and by failure to isolate the HVAC.

A probabilistic approach based on the event tree (ET) models was also used for PIEs related to some systems of the tritium plant. Comparison between the results of the PIE-PIT and the ET probabilistic approach confirmed that the selection of the first two bounding accident sequences above was correct. The third sequence has not been treated probabilistically.

Fire-impact analysis for the tokamak and tritium buildings. The aim of the fire hazard analysis was to demonstrate that environmental releases of tritium, as a consequence of the worst conceivable fire, remain within the limits specified by the project release guidelines. The fire severity is based on an inventory of combustible materials,

References

[3.25] T. Pinna, F. Gravanti and G. Cambi, *JET data collection on component malfunctions and failures of neutral injectors and power supply systems,* ENEA Internal Report FUS-TN SA-SE-R-121 (2004)

[3.26] T. Pinna et al., *Collection and analysis of data related to fusion machines (JET and TLK) operating experience on component failures*, ENEA Internal Report FUS-TN SA-SE-R-058 (2003)

[3.27] M.T. Porfiri and S. Paci, *STARDUST experiments for active dust extraction from ITER vacuum vessel*, ENEA Internal Report FUS-TN SA-SE-R-112 (2004)

[3.28] M.T. Porfiri and L. Verdini, *Set up of the STARDUST facility for the exchange flow experiments,* ENEA Internal Report FUS-TN SA-SE-R-98 (2004)

[3.29] T. Pinna, C. Rizzello and R. Caporali, *In-depth analysis of selected ITER accident sequences: relevant events for tritium plant*, ENEA Internal Report FUS-TN SA-SE-R-096 (2004)

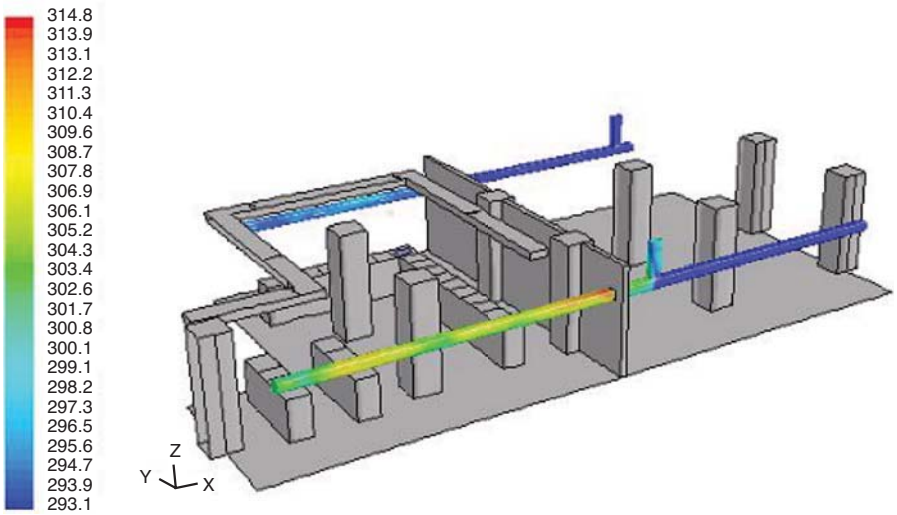

Fig. 3.31 - Maximum temperature in the ventilation ducts of ANS and SDS room and confining zone (long-term storage room)

defined by fire load, in each area of the plant. The temperatures reached by the process components were evaluated by the standard ISO-834 curve and compared with the temperatures specified by the design conditions, as a simplified screening criterion. The comparison showed that the temperatures were close to exceeding those of the design conditions and that several components could fail in a fire accident. As fire-severity categorisation is too conservative, fire-impact analyses are performed to get a more accurate evaluation of the consequences. A detailed fire-impact study [3.30] was therefore done for a number of representative rooms and areas (storage and delivery system [SDS] and analytical system [ANS], power distribution and control cubicles, standby-ventilation detritiation system/dedicated regeneration system [S–VDS/DRS], tritium monitoring, vacuum pumping system [VPS], port cell, drain tank area, gallery) to determine whether a fire can lead to tritium release. The simplified Fire Dynamic Simulation (FDS) model was used. The first evaluation gave the ANS and SDS room as being the most critical. The fluid dynamic analysis of the fire evolution was performed by means of the FLUENT code, which simulates the fire phenomenon in a more detailed and precise form. Although the analyses were very conservative, they demonstrated that the consequences of a fire accident (fig. 3.31) would be less severe than those resulting from a classical fire analysis (in which oxygen is never exhausted, all the combustible materials are supposed to burn and flashover conditions are assumed). The classical fire analysis results in an overestimation of the temperatures and thermal loads on structures and equipment. One of the parameters included in the fire analysis performed by the FDS is the ability to ignite; hence, as all the materials were considered to be practically flameproof, even a strong source of ignition would not be capable of priming a fire.

Another result was that the spread of fire can often be limited by oxygen depletion inside the rooms. The flow rate of ventilation in the range of one air change/hour is not sufficient for a fire to develop inside a sealed room.

Table 3.III - Comparison of EVITA experimental results and CONSEN simulation results; error=(C-E)/E

TEST	LIQUID MASS (g)			ICE MASS (g)		
	Calcul.	Experim.	Error	Calcul.	Experim.	Error
6.1	0	19	-	387	345	12%
6.22	1299	1370	-5%	280	274	2%
6.3	1913	1980	-3%	576	510	13%
6.4	4257	4350	-2%	264	340	7%
6.51	120	53	126%	215	250	-14%
6.61	1064	1017	5%	425	440	-3%
6.7	1431	1385	3%	156	160	-7%
6.8	3931	3750	4%	233	330	-29%
6.9	0	0	0	184	191	-4%
6.10	0	0	0	141	157	-10%
6.11	0	6	-	327	367	-11%

3.9.5 Validation of computer codes and models

Work continued on the validation, verification and qualification of the computer codes CONSEN, PACTITER and ANITA-2000 used for the ITER safety assessment.

CONSEN. The CONSEN code [3.31] was validated against the cryogenic tests performed at the experimental facility EVITA (CEA laboratories-France). CONSEN is well able to simulate steam condensation on a cryoplate. The code was validated against eleven tests in 2004. When the boundary conditions are accurately defined, the trends of temperature, pressurisation and the mass of ice formation agree with the experimental results. Sometimes, the difficulty in getting information on heat exchange in the cryoplate cooling loop, where nitrogen is present in two phases (liquid and gas), leads to discrepancies between the code and the experimental results. The heat removed from N_2 in tests with cold walls (tests 6.51, 6.61, 6.7 and 6.8) is greater than in the experiments. Agreement was generally good when calculating the final pressure and was also satisfactory for the residual liquid masses, apart from test 6.51 (table 3.III).

Table 3.IV - Best fit results

Test	T(°C)	Re	CORELE Release rate [mg/(dm^2 xmonth)]	PACTITER Release rate [mg/(dm^2 xmonth)]
				POROS=0.8, $pH_{25°C}$=7.9
2004-01 SE1	150	5.93×10^4	22.0	19.40
2004-01 SE2	150	8.57×10^4	36.0	24.50
	150	3.45×10^5	-	31.00
				POROS=0.4, $PH_{25°C}$=9.2
2004-03 SE3	100	3.62×10^4	0.8	1.05
2004-04 SE4	100	5.76×10^4	2.8	1.55
	100	2.11×10^5	-	4.48

PACTITER. The PACTITER v2.1 code was used for simulations of the CORELE experiments [3.32]. The objective was to determine the stainless steel (SS316L) release rate under the thermal-hydraulic and chemical conditions of the primary cooling loops. The results showed an increase in release rate with fluid temperature T, fluid velocity and the parameter POROS, i.e., porosity of the oxide layer on the inner surface of the tube. Temperature has a strong influence; simulations at T=100°C provided lower material release rates than those calculated at T=150°C (factor of ~10), in fair agreement with the experiments. With reference to fluid velocity instead calculated results were in disagreement with experiments: the release rate in the experiments decreases with increasing fluid velocity, but according to the code it increases. In fact, the CORELE tests that were carried out at a fluid velocity of 4 m/s were characterised by a lower Re number than those at v=1 m/s. The reason for this was the change in the tube geometry (presence of the Zircalloy insert placed in the tube to overcome the reduced fluid flow rate). The calculated SS316L release rates agreed fairly well with the experimental results using the same Re Number as correlation factor.

It was impossible to get a full match between measured pH and Li content and the corresponding input data for code simulations. The best fit with the CORELE experiments was obtained with $pH_{25°C}$=9.2 for tests at T=100°C, and with $pH_{25°C}$=7.9 for tests at T=150°C. The porosity of the oxide layer on the inner surface of the tube (POROS) is important, as already demonstrated in previous CORELE test simulations. Two values were used: 40% and 80%. The simulation results showed a better agreement with experiments by adopting POROS = 0.8 for T=150°C and POROS=0.4 for T=100°C. See table 3.IV for details.

References

[3.30] C. Rizzello, M.T. Porfiri and P. Roccetti, *Fire hazard analysis in ITER buildings,* ENEA Internal Report FUS-TN SA-SE-R-117 (2004)

[3.31] G. Caruso and M.T. Porfiri, *EVITA cryogenic tests with gas injection: post-test calculations,* ENEA Internal Report FUS-TN SA-SE-R-119 (2004)

[3.32] L. Di Pace, *CORELE 2004 tests simulation,* ENEA Internal Report FUS-TN-SA-SE-R-122 (2004)

ANITA. A new validation effort was performed for the ANITA neutron activation code [3.33, 3.34]. The decay heat measurements on fusion-relevant materials (cobalt, copper, iron, Inconel-600, nickel, nichrome (NiCr), tantalum, titanium, SS-304, SS316) irradiated by 14-MeV neutrons at the JAERI fusion neutron source were analysed by ANITA with EAF-2003 data and FENDL/A-2 nuclear data libraries. JAERI provided the source neutron-energy spectrum and intensity as well as the 175-n Vitamin-J energy-group structure flux distribution for each one of the material samples. The decay-heat calculation and experimental results were compared. The general conclusion from the calculation/experiment comparison is that EAF-2003 generally provides a better agreement with the experiments than FENDL/A-2. The photon and electron decay-heat measurements from the Frascati FNG were compared with ANITA/FISPACT results, based on EAF-2003 data, for Mo, Cu, Hf, Mg, Ni, Cd, Sn, Re, Ti, W, Ag, and Al. The impact of different activation libraries (i.e., EAF-99, EAF-2003 and FENDL/A-2) on the ANITA-2000 results was also assessed. The decay-data library FENDL/D-2 was used for the calculations. The ANITA-2000 and FISPACT calculations (using the EAF-2003 activation library) for both activity and gamma-beta decay heats differ by less than 1% for all the materials except Hf and Sn. Some slight differences in the decay data used in the calculations (life-times, gamma energies, etc.) and the different numerical treatment of the nuclear chains are responsible for the observed discrepancies.

The SCALENEA-1 calculation sequence developed to evaluate various nuclear response functions includes three main steps: processing of nuclear data (from evaluated nuclear data files) to produce master and working data libraries (problem dependent); analysis of radiation (n,γ) transport to produce neutron/gamma spectra and reaction rates; post-processing of radiation transport results to obtain various response functions (i.e., physical parameters, such as neutron activation data). The new updated calculation approach SCALENEA-1 uses the VITENEA-J library for radiation transport analyses and either FISPACT-2003 or ANITA-2000 with the EAF-2003 neutron activation library for activation calculations [3.35-3.37].

3.9.6 Safety-relevant activation calculations

Stainless steel SS316 LN-IG inventories related to wet zones of the ITER first wall and blanket coolant loops were updated to support the activated corrosion product (ACP) assessment for the primary heat transfer system (PHTS). The impact of the cobalt content in SS36 and of the different irradiation scenarios on the ACP radioactive inventories was analysed. A reference value (i.e., 0.05 wt%) and a higher value (i.e., 0.1 wt%, and a modified Fe wt% content for balance) were considered for the cobalt content. The steel activation of the PHTS cooling pipe (outboard zones) increased (both at the end of the irradiation and for one day's cooling time) by about 5% and the cobalt content increased from 0.05% to 0.1%. The highest increase is for the zones far from plasma [3.38].

The activation characteristics of some in-vessel outboard zones/materials were compared with those included in Vols. III and V of the Generic Site Safety Report (GSSR). No significant differences (within 1%) were found between the results of ANITA and FISPACT for specific activity, decay heat and clearance index, at shutdown and up to about 100 years' cooling time, when using the same activation data library. For contact dose rates the differences were up to 12%. Higher discrepancies were found for longer cooling times. When using the same activation code, there were no significant differences (less than 5%) between the results obtained with the EAF-99 and EAF-2003 libraries at shutdown and for short cooling times (lower than one year), while the discrepancies increased for longer cooling times. Some differences were found for the FENDL/A-2 library for all the activation parameters, particularly at shutdown and for short cooling times. The highest discrepancies were for zones/materials far from the plasma zone. A check test was made only for a few materials (outboard in-vessel FW/BL zones) and only for general activation parameters (no isotope inventories). However, it would seem that the inventory results contained in the GSSR, based on EASY-99 and ANITA-2000 (with the EAF-99 activation library), are reliable, at least for short cooling times.

3.9.7 Power Plant Conceptual Study

Helium-cooled divertor. Further analyses performed with the use of a 3D model and the ABAQUS code confirmed not only the previous results obtained with an axisymmetric model [3.39] but also the substantial validity of the proposed solution [3.40, 3.41]. Analysis of the decay dose of a divertor manufactured using DENSIMET (W-Cu-Ni alloy) as structural material showed that the alloy does not affect the 100-year dose of divertor waste (fig. 3.32). Material has been supplied to manufacture a two-element module for testing in a helium facility.

Safety analyses. Several representative accident scenarios for Models C and D fusion reactors were specified for deterministic assessment [3.42]. Functional failure mode and effects analyses were performed for the two models. Starting from a plant functional breakdown, the failures of each system were analysed at functional level. A set of expected PIEs was selected. The possible evolution of the accident was pointed out. The main systems and subsystems involved in the different sequences were identified, and deterministic analyses were carried out to verify the resistance of the containments. Radioactive-inventory mobilisation and possible environmental release were also qualitatively defined. The representative accident scenarios that could challenge the containments or result in radioactive mobilisation are: loss of flow in one primary cooling loop with a consequent in-vessel loss LOCA; generalised loss of heat sink; in-vessel LOCA; ex-vessel LOCA with consequent in-vessel LOCA; interface LOCA between FW and blanket for Model C.

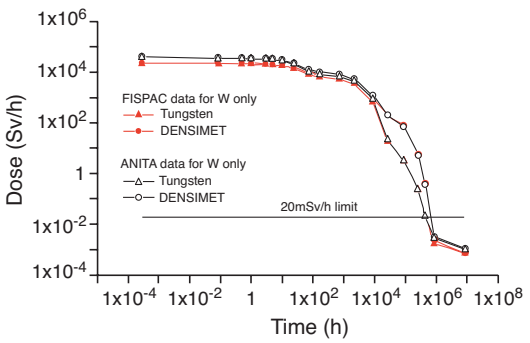

Fig. 3.32 - Dose comparison for tungsten and DENSIMET divertors

References

[3.33] D.G. Cepraga, G. Cambi and M. Frisoni, *ANITA and EASY activation code packages: 2004 validation effort, EFDA task No. TW4-TSS-SEA5.5, deliverable D1 - final report,* ENEA Internal Report FUS-TN- TN-SA-SE-R-114 (2004)

[3.34] G. Cambi, D.G. Cepraga and M. Frisoni, *Experimental fusion material photon and electron decay heat measurements: its use for activation codes validation*, 23rd Symp. on Fusion Technology - SOFT23 (Venice 2004)

[3.35] M. Frisoni, D.G. Cepraga and G. Cambi, *VITENEA-J, AMPX 175-N,42-gamma multigroup X-sect. library for nuclear fusion applications*, NEA Data Bank Program NEA-1703, OECD Nuclear Energy Agency (Paris 2004)

[3.36] G. Panini et al., *VITENEA-E, AMPX 174-N,38-gamma multigroup X–sec. library for multidimensional radiation transport and dose evaluation,* NEA Data Bank Program NEA-1702, OECD Nuclear Energy Agency (Paris 2004)

[3.37] D.G. Cepraga, M. Frisoni and G. Cambi, *Vitenea-J: a multigroup coupled (175 n - 42 γ) cross-section library in AMPX format for nuclear fusion applications,* ENEA Internal Report FIS/MET/2004/2 (2004)

[3.38] D.G. Cepraga, G. Cambi and M. Frisoni, *Summary report on the 2004 ENEA 1D-Sn neutronics and activation calculations for ITER, EFDA task No. TW4-TSS-SEA4.1, deliverable D1 - final report*, ENEA Internal Report FUS-TN- TN-SA-SE-R-115 (2004)

[3.39] A. Pizzuto et al., *HETS performances in He cooled power plant divertor,* Presented at 23rd Symp. on Fusion Technology – SOFT23 (Venice 2004)

[3.40] P. Norajitra et al., *The European development of helium-cooled divertors for DEMO*, presented at XX IAEA-FEC 2004 (Vilamoura 2004)

[3.41] D. Maisonnier et al., *The European Power Plant Conceptual Study*, presented at 23rd Symp. On Fusion Technology – SOFT23 (Venice 2004)

[3.42] T. Pinna and R. Caporali, *Identification of accident sequences for the power plant conceptual study Models C and D*, ENEA Internal Report FUS-TN SA-SE-R-103 (2004)

ORE Assessment. The latest information obtained from ITER R&D activities (mainly for fuelling and vacuum pumping) was exploited to prepare an outline design of the fuel cycle system [3.43], and all the details required for an occupational radiation exposure (ORE) assessment were provided.

The assessment of the ORE for the fuel cycle systems of Models A and B was updated [3.44] with reference to the fuelling, vacuum pumping and blanket tritium recovery systems. The impact of the design changes on estimated collective worker doses was determined and analysed. The cumulative impact of the design changes on each plant model is about a 50% reduction in estimated annual maintenance dose. The largest dose reduction occurs in the vacuum pumping system, for both plant models. The second largest reduction is in the fuelling system, owing almost exclusively to pellet injection design changes. Some changes were also introduced in the dose assessment methodology, based on the work-effort estimating rule, developed from analysis of JET ORE data.

A proposal was made to update the occupational dose targets of the General Design Requirements Document (GDRD) [3.45]. Starting from an analysis of the GDRD target evolution since the second stage of the PPCS and taking into account the update of the ORE for the fuel cycle systems of Models A and B, it was proposed to modify the share of the different contributions to the total GDRD target appointed to the fuel cycle systems, keeping the total unchanged (200 p–mSv/a). The contributions of the fuel cleanup systems (10 p-mSv/a) and isotope separation system (10 p-mSv/a) remain unchanged. The proposed modifications are:

- fuelling system from 60 p-mSv/a down to 20 p-mSv/a;
- vacuum pumping system from 60 p-mSv/a up to 100 p–mSv/a;
- blanket tritium recovery system no change (60 p-mSv/a).

Watching brief activities in the field of radioactive waste management. The current status of decommissioning worldwide, the different strategies used, the relative problems and costs have been investigated and reported in detail [3.46].

The decommissioning problem will increase markedly within a decade and is going to become an important issue for the nuclear industry. At present, of the 600 research reactors built and operated all over the world, 400 have been either shut down, decommissioned or are under decommissioning. On the other hand, out of the 500 or so nuclear power plants that have been constructed worldwide, 102 are either under or destined for decommissioning.

Decommissioning policies, strategies and timescales can vary from country to country. The generally accepted timescale for decommissioning as proposed by the International Atomic Energy Agency (IAEA) refers to three stages:

1. immediate dismantling of the facility;
2. safe storage or deferred dismantling and
3. eventual entombment of the facility.

Each stage can be defined by two characteristics: the physical state of the facility and the surveillance required to maintain such a state.

There are two general approaches to carrying out the decommissioning of a nuclear facility, and one or the other has a substantial effect on the project management:

- The licensee performs the decommissioning with in-house resources supplemented by specialist contractors as required.
- The licensee contracts an experienced outside organisation to take charge of the decommissioning activities, while the licensee does the general overseeing and planning.

3. Technology Programme

Major concerns in any decommissioning programme are to safeguard the health and safety of the workers and general public and to protect the environment. However, the risk of public exposure and environmental impact is lower during plant decommissioning than when the plant is in operation. This has a simple sound basis: once the spent fuel has been removed, the radioactivity inventory available for release to the environment is reduced. All the same, a significant effort is made in all nuclear operations to keep the exposure as low as reasonably achievable (ALARA).

One of the major issues related to safety and environmental impact is waste management, with its implications of unconditional release and material recycling. Decommissioning waste is distinguished by its huge amount and by the fact that it is only slightly or non-radioactive (99% of the mass contains only 1% of the total activity). As undue costs, environmental impact and problems of public acceptability have to be avoided when managing waste, a solution could be either to clear material with negligible residual radioactivity from regulatory control or to promote recycling of the material when the level of radioactivity is acceptable to the nuclear industry.

References

[3.43] L. Di Pace and D.K. Murdoch, *Outline design of the PPCS Models A and B fuel cycle systems,* ENEA Internal Report FUS-TN-SA-SE-R-101 (2004)

[3.44] A. Natalizio and L. Di Pace, *Worker dose assessment for PPCS Models A & B fuel cycle systems*, ENEA Internal Report FUS-TN-SA-SE-R-109 (2004)

[3.45] A. Natalizio and L. Di Pace, *Review of GDRD worker dose targets for PPCS fuel cycle systems*, ENEA Internal Report FUS-TN-SA-SE-R-116 (2004)

[3.46] L. Di Pace, *Ongoing activities related to the decommissioning of fission power plants which may be of interest for fusion waste. Intermediate Report,* ENEA Internal Report FUS-TN-SA-SE-R-110 (2004)